Point Blue Conservation Science

National Marine Sanctuaries

National Oceanic and Atmospheric Administration · U.S. Department of Commerce · NOAA

Ocean Climate Indicators Status Report – 2019

Black-footed Albatross. Photo by Mojoscoast, ACCESS / NOAA / Point Blue

This page
was intentionally
left blank

Ocean Climate Indicators Status Report – 2019

Final Report – July 2020

Prepared by

Point Blue Conservation Science
Meredith Elliott
Pete Warzybok
Jaime Jahncke, PhD

Cordell Bank National Marine Sanctuary
Danielle Lipski

Greater Farallones National Marine Sanctuary
Jan Roletto

Suggested citation:
Elliott, M., Lipski, D., Roletto, J., Warzybok, P., and Jahncke, J. 2020. Ocean Climate Indicators Status Report: 2019. Unpublished Report. Point Blue Conservation Science Contribution No. 2320, Petaluma, CA.

*Corresponding author: melliott@pointblue.org

Website link:
http://www.accessoceans.org/wp-content/uploads/2020/07/Ocean_Climate_Indicators_Report_2019.pdf

ACKNOWLEDGEMENTS

We would like to thank our leadership Manuel Oliva, CEO, Point Blue Conservation Science, Dan Howard, Superintendent, Cordell Bank National Marine Sanctuary, Maria Brown Superintendent, Greater Farallones National Marine Sanctuary, and Bill Douros, Regional Director, West Coast Region, Office of National Marine Sanctuaries. We also want to acknowledge Chris Barr and Gerry McChesney from the U.S. Fish and Wildlife Service and the Farallon Islands National Wildlife Refuge for partnering with Point Blue to monitor wildlife on the Farallon Islands, The Southeast Farallon sea surface temperature and sea surface salinity data are provided by the Shore Stations Program with funding provided by the California Parks and Recreation, Department of Boating and Waterways, award # CA DPR-C1370020; these data are collected by research personnel with Point Blue Conservation Science.

We thank the California Department of Public Health (Vanessa Zubkousky-White) for contributing phytoplankton data, the Institute of Ocean Sciences (Moira Galbraith) for helping process zooplankton samples collected during ACCESS cruises, and Ben Saenz for processing the acoustics data. The Estuary and Ocean Science Center (under the guidance of Frances Wilkerson and Sarah Blaser) provided nutrient analyses, and the U.C. Davis Bodega Marine Laboratory (with Nancy Foster Scholars Carina Fish and Kate Hewett, under the direction of Tessa Hill and John Largier) conduct ocean acidification monitoring; we are grateful to these academic institutions and staff for these new avenues of research.

Funders of the Applied California Current Ecosystem Studies (ACCESS) partnership include Cordell Bank National Marine Sanctuary, Greater Farallones National Marine Sanctuary, the Elinor Patterson Baker Trust, Battery Powered, Bently Foundation, Bonnell Cove Foundation, Boring Family Foundation, California Sea Grant, California Dept. of Fish and Wildlife, Central and Northern California Ocean Observing System (CeNCOOS), Cordell Marine Sanctuary Foundation, DJ&T Foundation, Echoview Software Pty Ltd, Greater Farallones Association, Faucett Catalyst Foundation, Firedoll Foundation, Giles W. and Elise G. Mead Foundation, Gordon and Betty Moore Foundation, Hellman Family Foundation, Marisla Foundation, McCaw Family Foundation, Monterey Bay National Marine Sanctuary, Moore Family Foundation, National Fish and Wildlife Foundation, National Marine Sanctuary Foundation, Oikonos Ecosystem Knowledge, Pacific Life Foundation, Resources Legacy Fund Foundation, Restoration Center (NOAA), Richard Grand Foundation, Office of National Marine Sanctuaries, Sanctuary Supporters LLC, The Nature Conservancy, Thelma Doelger Trust for Animals, The Volgenau Foundation, and Point Blue Anonymous Donors. Results in this report would not be possible without Point Blue staff, interns and volunteers.

EXECUTIVE SUMMARY

The purpose of this report is to inform managers and policy-makers about wildlife responses to changes in ocean conditions and to make this information available to other researchers and the public.

This report builds off two reports: *Ocean Climate Indicators: A Monitoring Inventory and Plan for Tracking Climate Change in the North-central California Coast and Ocean Region* (Duncan *et al*. 2013), which prioritized indicators for monitoring; and the *Climate-Smart Adaptation for North-central California Coastal Habitats* report (Hutto 2016), which provided strategies to ensure ecosystem-based management and the long-term viability of the important species and habitats in this region. Other indicators (e.g., basin-scale climate indices, sizes of euphausiids, at-sea distributions of seabirds and marine mammals) that were readily available and provide a more comprehensive picture of regional ocean conditions were also included. The information we collect is available upon request to potential collaborators and is included in the Central and Northern California Ocean Observing System (CeNCOOS) Data Portal (data.cencoos.org). The report is available at www.accessoceans.org and www.sanctuarysimon.org.

We looked at numerous climate indicators to determine the health of the ecosystem and define annual responses by the ecosystem. To determine the health of the ecosystem we used data collected through the ACCESS project and data collected through NOAA climate monitoring projects. Here we describe the ecosystem conditions and responses in 2019.

NOAA and other marine research institutions' data used as climate indicators and ecosystem responses include: Southern Oscillation Index (SOI); Pacific Decadal Oscillation (PDO); North Pacific Gyre Oscillation (NPGO); Alongshore wind intensity; Upwelling Index & Spring transition date; Sea surface height; Sea surface temperature; Sea surface salinity; Chlorophyll a concentrations; Seabird breeding success; Seabird population trends on SE Farallon Island; Seabird timing of breeding; and Seabird diet.

ACCESS data used as climate indicators and ecosystem responses include: Ocean acidification (as measured by the aragonite saturation state); Dissolved oxygen & hypoxia; Nutrient concentrations; Phytoplankton community composition; Zooplankton community composition; Copepod composition; Pteropod composition; Euphausiid biomass; Euphausiid size & age class; and Abundance & distribution of five top-level predators (Cassin's auklet, Common murre, Brandt's cormorant, Blue whale, and Humpback whale) as indicator species.

Physical ocean climate indicators illustrated poor ocean conditions (i.e., warm waters, fewer nutrients) for most of 2019, with improving conditions in the latter part of the year. Climate indices, such as the Southern Oscillation Index (SOI) and the North Pacific Gyre Oscillation (NPGO), indicated warm, low productivity conditions for the year. Alongshore winds were weak in the early months, followed by average to strong winds. Upwelling indices were mixed depending on the source, showing weak upwelling (on a local scale) and either strong upwelling or pulses of upwelling and relaxation throughout the year (on a regional scale). Sea surface heights were elevated throughout the year, suggesting downwelling conditions.

Spring transition date was late. Sea surface temperature showed an overall warm regime for the year, with a local buoy showing cooler conditions in the fall months. Sea surface salinity values were above average in the early months, followed by average values; nutrient concentrations were low except in May.

Biological ocean climate indicators echo results from the physical indicators. Starting at the base of the marine food web, phytoplankton abundance (as indicated by chlorophyll a concentrations) showed low to average abundances for the first half of the year. Phytoplankton community results indicated a diatom-dominated community in early 2019, followed by a dinoflagellate-dominated community. Zooplankton community composition results from the ACCESS hoop net tows are not yet available for 2016-19; we show results from 2004-15. The most recent results from 2015 reflect overall high abundances of zooplankton compared to warm, poor productivity years (e.g. 2004-06), particularly for copepods and the "other" category (which is mostly comprised of gelatinous species). We examined copepods, pteropods, and euphausiids in more detail, as these are important low- to mid-trophic level species in the ecosystem. Euphausiid biomass (as measured by acoustics) is not yet available for 2019; warm water conditions generally show a decline in the percentage of adult stages, although 2019 (a warm year) showed relatively high abundances of adult euphausiids found in ACCESS Tucker trawl tows. Additionally, adult euphausiids are larger in cold water years (e.g. 2007-13) and smaller in warm water years (e.g. 2005-06, 2014-16); adults in 2019 were larger than adults in 2018, indicative of the transition from the 2014-2016 North Pacific marine heat wave.

The top-level predators in our region are represented by three resident breeding seabirds, Cassin's auklet, common murre and Brandt's cormorant, and two migrant whales, blue and humpback. Cassin's auklet, a zooplanktivorous seabird, was observed foraging over Cordell Bank in 2019; the average egg laying date was slightly later for this species and experienced anomalously low breeding success. An omnivorous seabird species, the common murre, foraged across the shelf in 2019, had a slightly later egg laying date, experienced very low breeding success, and consumed mostly anchovy and sardine. Brandt's cormorants are piscivorous and were observed in low numbers near Southeast Farallon Island (SEFI) and nearshore waters in 2019. This species had a slightly later start to breeding, experienced somewhat above-average productivity, and consumed mostly anchovy in 2019. For marine mammals in 2019, humpback whales were observed in high numbers; they were spotted over the continental shelf. Blue whales were observed in relatively low numbers in 2019 compared to the previous year; they appeared near Cordell Bank in May and September. Both species showed peak numbers in September 2019.

In summary, most physical indicators showed poor conditions, while the biological indicators available for the year showed mixed results (Table 1).

Table 1. Summary of 2019 conditions as determined by physical and biological indicators.

Indicator Name (*scale*)	2019 Conditions
Physical Indicators	
Southern Oscillation Index	Poor
Pacific Decadal Oscillation	Average
North Pacific Decadal Oscillation	Poor
Wind	Poor
Sea surface height	Poor
Upwelling (BB) – *local*	Poor
Upwelling (PFEL) – *regional*	Good
Upwelling (CUTI) – *regional*	Average
Spring transition (BB) – *local*	Good
Spring transition (PFEL) – *regional*	Good
Sea surface temperature (BB) – *local*	Average
Sea surface temperature (SEFI) – *local*	Poor
Sea surface temperature (Satellite) – *regional*	Poor
Sea surface salinity	Average
Aragonite saturation	Poor
Dissolved oxygen	Average
Nitrates (NO_3) and Nitrites (NO_2)	Poor
Phosphates (PO_4)	Poor
Silicates (Si)	Poor
Biological Indicators	
Chlorophyll a	Good
Phytoplankton composition	Poor
Zooplankton composition	Data not available
Copepods	Data not available
Pteropods	Data not available
Euphausiids – Acoustics	Data not available
Euphausiids – Age classes	Good
Euphausiids – Adult sizes	Average
Cassin's auklet – at-sea numbers	Poor
Cassin's auklet – egg laying date	Average
Cassin's auklet – breeding success	Poor
Cassin's auklet – diet	Data not available
Common murre – at-sea numbers	Average
Common murre – egg laying date	Average
Common murre – breeding success	Poor
Common murre – diet	Poor
Brandt's cormorant – at-sea numbers	Poor
Brandt's cormorant – egg laying date	Average
Brandt's cormorant – breeding success	Good
Brandt's cormorant - diet	Good
Humpback whale – at-sea numbers	Good
Blue whale – at-sea numbers	Average

TABLE OF CONTENTS

INTRODUCTION

The Applied California Current Ecosystem Studies (ACCESS) is a partnership between a non-profit science organization, Point Blue Conservation Science, and a Federal agency, NOAA, to inform management in support of marine wildlife conservation in north-central California, including Cordell Bank National Marine Sanctuary (CBNMS), Greater Farallones National Marine Sanctuary (GFNMS), and the northern portion of Monterey Bay National Marine Sanctuary (MBNMS; Figure 1). ACCESS conducts coordinated private and government research at an ecosystem scale to support management of a healthy marine ecosystem in the region. This includes integrated, collaborative, and multi-disciplinary research to monitor distribution, abundance and demography of marine wildlife in the context of underlying physical and biological oceanographic processes.

This reporting effort builds off two reports: *Ocean Climate Indicators: A Monitoring Inventory and Plan for Tracking Climate Change in the North-central California Coast and Ocean Region* (Duncan *et al*. 2013), which prioritized indicators for monitoring; and the *Climate-Smart Adaptation for North-central California Coastal Habitats* report (Hutto 2016), which provided strategies to ensure ecosystem-based management and the long-term viability of the important species and habitats in this region. Other indicators (e.g., basin-scale climate indices, sizes of euphausiids, at-sea distributions of seabirds and marine mammals) that were readily available and provide a more comprehensive picture of regional ocean conditions were also included. The information we collect is available upon request to potential collaborators and is included in the Central and Northern California Ocean Observing System (CeNCOOS) Data Portal (data.cencoos.org). The report is available at www.accessoceans.org and www.sanctuarysimon.org.

Data collected by ACCESS are used to inform effective management and conservation of resources in national marine sanctuaries. Some of the issues we aim to address include:

1) Wildlife conservation to improve management of marine wildlife and their food webs;
2) Ocean zoning to guide human uses to provide protection of the marine ecosystem by identifying biologically rich, persistent and ephemeral areas;
3) Climate change to document effects on the ecosystem and inform climate-smart conservation policy and management;
4) Ocean acidification to document changes in water properties and assess biological responses; and
5) Ecosystem indicators to assess responses to climate variability and produce long-term data to inform ecosystem-based management approaches.

ACCESS is a long-term monitoring project with proven applicability to inform urgent management concerns and at the same time has been adaptable to gathering information on emerging issues and providing data for changes in jurisdictions. In June 2015, NOAA expanded the boundaries of CBNMS and GFNMS, which more than doubled the size of both sanctuaries by extending boundaries north to Manchester Beach in Mendocino County (for GFNMS) and west to include important subsea features on the continental slope for both CBNMS and GFNMS. As the sanctuaries were planning to expand, so did the study area of ACCESS. In 2014, four survey lines were added to the proposed expansion area, now part of the sanctuaries, to collect baseline information in the northern areas, and these lines

remained part of the ACCESS study area in 2015; these new lines are sampled in years when we are granted ship time on larger NOAA research vessels or receive additional funding.

The purpose of this report is to inform managers and policy-makers about wildlife responses to changes in ocean conditions and to make this information available to other researchers and the public. The indicators shown in this report cover different spatial scales, including basin-scale (Pacific Ocean, or sometimes restricted to the North Pacific Ocean), regional scale (north-central California, roughly Bodega Bay to Half Moon Bay), and local scale (measurements, samples, or observations obtained at certain locations within the north-central California region). We present data collected during the ACCESS at-sea surveys which have been conducted 3-4 times a year since 2004. These data include phytoplankton composition, zooplankton composition, euphausiid abundance from hydroacoustics, and at-sea observations of seabirds and marine mammals. We have also compiled a variety of datasets to look at long-term trends; these include climate and upwelling indices, sea surface temperature and salinity measured from the Farallon Islands, buoy data (winds, sea surface temperature), satellite data (sea surface temperature and height, and phytoplankton abundance), and seabird data (productivity and timing of breeding) on Southeast Farallon Island. Please refer to the Appendix to find more details on each indicator. While some datasets have been updated through this year, not all 2019 data are available as samples and data are still being processed. This report summarizes the analysis available, up to and including the 2019 field season for some metrics. For each metric, the most recent data are presented first, followed by a description of the time series.

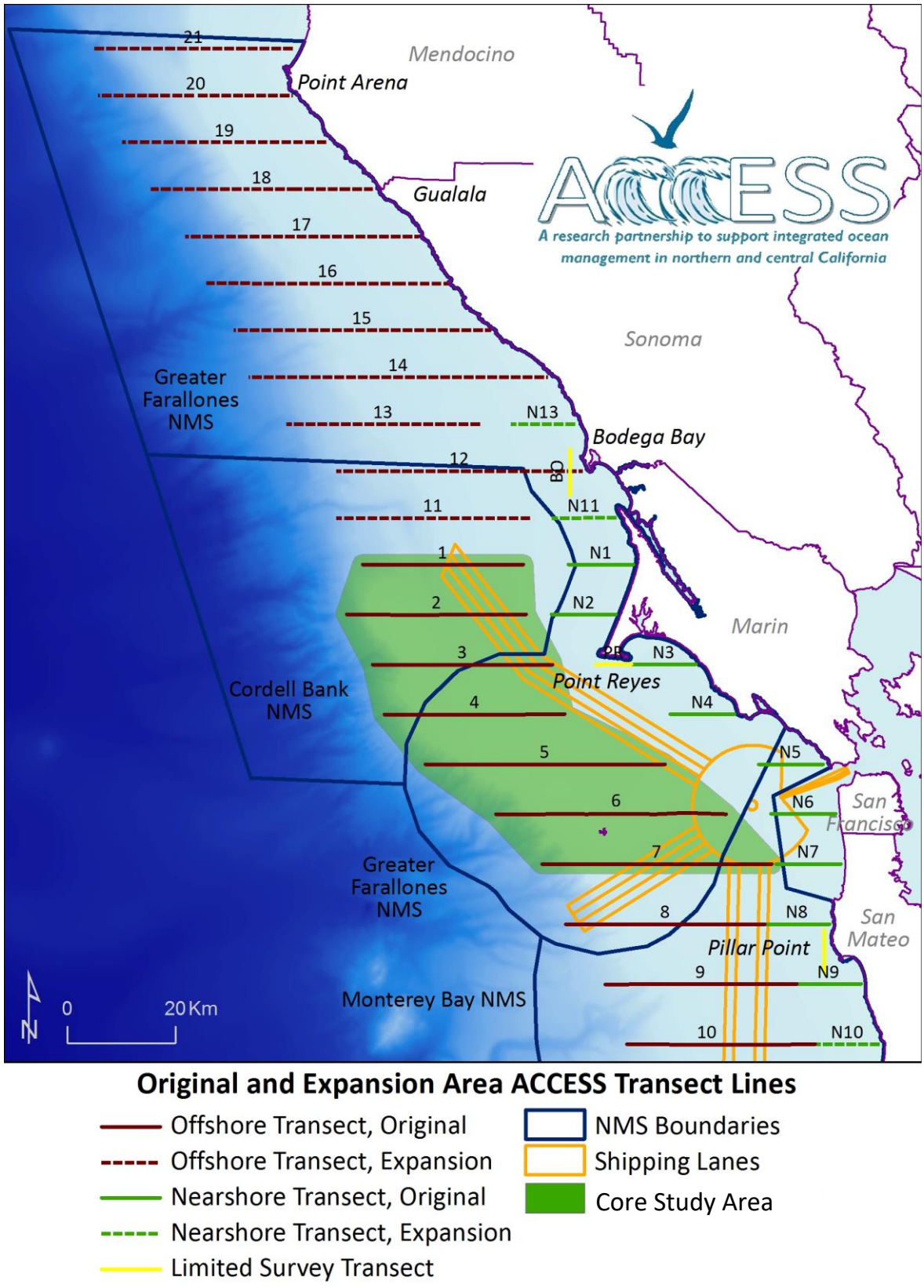

Figure 1. Applied California Current Ecosystem Studies (ACCESS) study area.

Physical Ocean Climate Indicators

Climate indices

Overview

NOAA developed several climate indices to understand climate patterns on the basin- scale. Each index measures different climate-ocean events (from El Niño/La Niña episodes to ocean circulation) to give a more comprehensive view of the ocean conditions in a given time period. The Southern Oscillation Index (SOI) is based on differences in standardized mean sea level pressure between Tahiti and Darwin, Australia. Negative SOI values indicate warm ocean conditions related to El Niño, and cold water conditions are shown in positive SOI values. The Pacific Decadal Oscillation (PDO) measures changes in surface water temperature in the North Pacific (from 20°N to the north pole) at inter-decadal patterns. Positive PDO values correspond to warmer ocean waters in the eastern Pacific, and negative PDO values correspond to cold waters. The North Pacific Gyre Oscillation (NPGO) measures changes in circulation of the North Pacific gyre, and is highly correlated with nutrients and overall ocean productivity. Negative NPGO values indicate warm water and poor conditions, while positive values correspond to productive conditions. See SOI, PDO, and NPGO sections in the Appendix for details on these data.

Southern Oscillation Index (SOI)

SOI values in 2019 showed warm water conditions (i.e. negative red bars) throughout the year (Figure 2). Warm waters were observed from 2004 through the first half of 2007, then from early 2009 through mid-2010, and then again in 2014 through mid-2016. Cold water conditions (i.e. positive blue bars) were observed from mid-2007 through early 2009, mid-2010 through 2011, 2013, and the last half of 2016 and 2017. For a list of recent El Niño events, visit https://ggweather.com/enso/oni.htm.

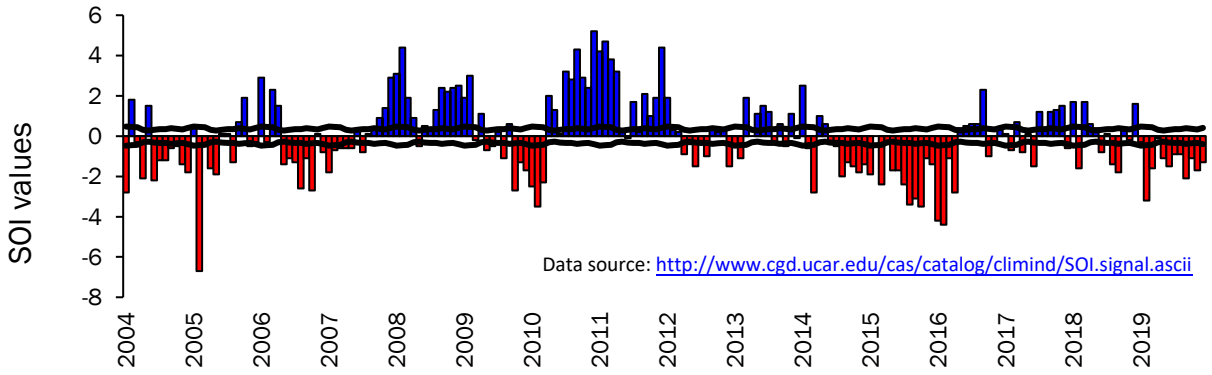

Figure 2. Southern Oscillation Index (SOI) values, 2004-19. Black lines represent ±99% confidence intervals around the long-term monthly means.

Pacific Decadal Oscillation (PDO)

PDO results for 2019 were not available at the time we wrote this report, so we can only show results through Sep 2018 (Figure 3). Warm water conditions (i.e. positive red bars) dominated the early years of this time series (roughly 2004-07), and from mid-2009 through mid-2010, and from 2014 through 2017. Cold water conditions (i.e. negative blue bars)

were more prominent from late 2007 through the end of 2009, and from mid-2010 through 2013. Cooler conditions may be returning as evidenced by the average values observed in 2018.

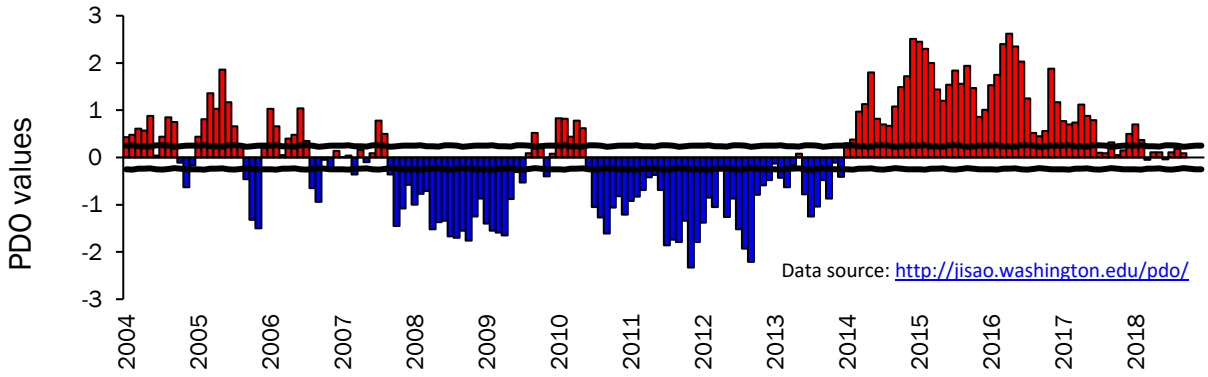

Figure 3. Pacific Decadal Oscillation (PDO) values, 2004–Sep 2018. Black lines represent ±99% confidence intervals around the long-term monthly means.

North Pacific Gyre Oscillation (NPGO)

NPGO values for most of 2019 indicate anomalously warm, poor productivity (i.e. negative red bars) conditions for the year (Figure 4). Warm water and poor productivity conditions were evident in 2005-06, and for most of the period from 2014 to present. Cold, productive conditions (i.e. positive blue bars) prevailed from 2007 through 2013.

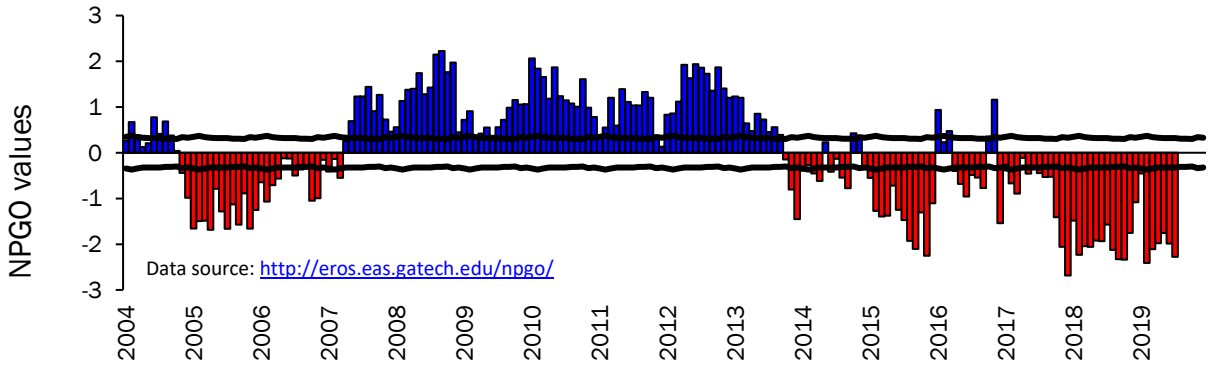

Figure 4. North Pacific Gyre Oscillation (NPGO) values, 2004–July 2019. Black lines represent ±99% confidence intervals around the long-term monthly means.

Winds, upwelling and sea surface height

Overview

Upwelling is a wind-driven process where coastal winds blowing parallel to the coast result in an offshore movement of surface water drawing deep, cold, nutrient-rich waters to the surface nearshore. The strength and periodicity of upwelling can have a significant effect on the marine ecosystem; periods of strong upwelling are normally alternated by relaxation events that allow for the spring bloom to occur. Historically, alongshore winds and upwelling values increase from March through June (both reaching a maximum in June), then decline

through the remainder of the year. In addition to wind and upwelling indices, sea surface height is an indicator of upwelling conditions. When sea surface height is low, this is an indication that winds have pushed surface waters offshore and upwelling is occurring. See the NOAA Bodega Bay buoy data, sea level height satellite data, NOAA PFEL Coastal Upwelling Indices, and CUTI sections in the Appendix for details on these data.

Winds

Local scale winds measured at the NOAA buoy 46013 were weak (i.e. positive red bars) for most of 2019, with short periods of strong northerly alongshore winds (i.e. negative blue bars) in July and the fall (Sep-Nov; Figure 5). There was moderate alongshore wind activity in 2004, followed by a lack of northerly winds in 2005-06. Strong, upwelling-producing winds dominated for most of 2007-13. Winds in 2014-16 were largely weak, while 2017-18 saw mostly moderate winds.

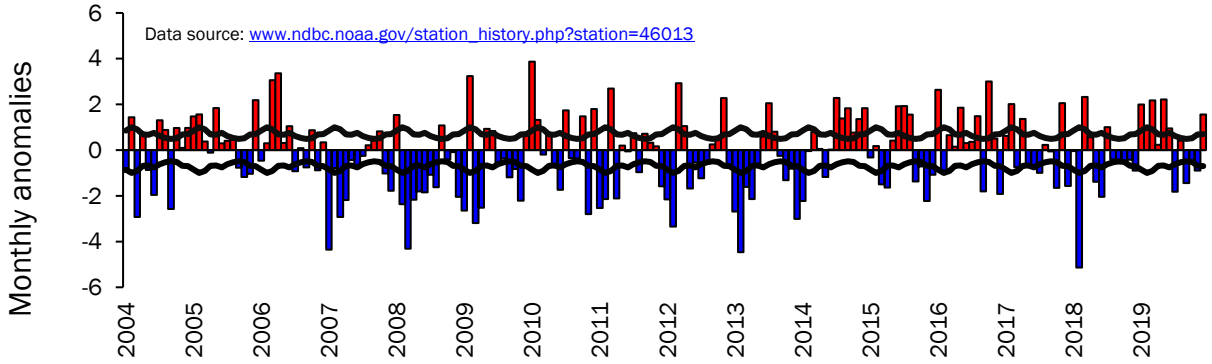

Figure 5. Monthly anomalies of alongshore winds, 2004–19. Black lines represent ±99% confidence intervals around long-term monthly means. Red bars indicate weak winds, and blue bars indicate strong winds.

Satellite Sea Surface Height

Regional sea surface height (SSH) measured from satellites in 2019 was high (i.e., positive red bars) and decreasing in the fall (Figure 6). High values observed in 2004-06 and 2009-2010 were associated with anomalous warm ocean conditions and El Niño. Low values typical of upwelling were dominant most of the time from 2007 to 2013. High values observed from 2014 to 2016 were associated with North Pacific heatwave and El Niño.

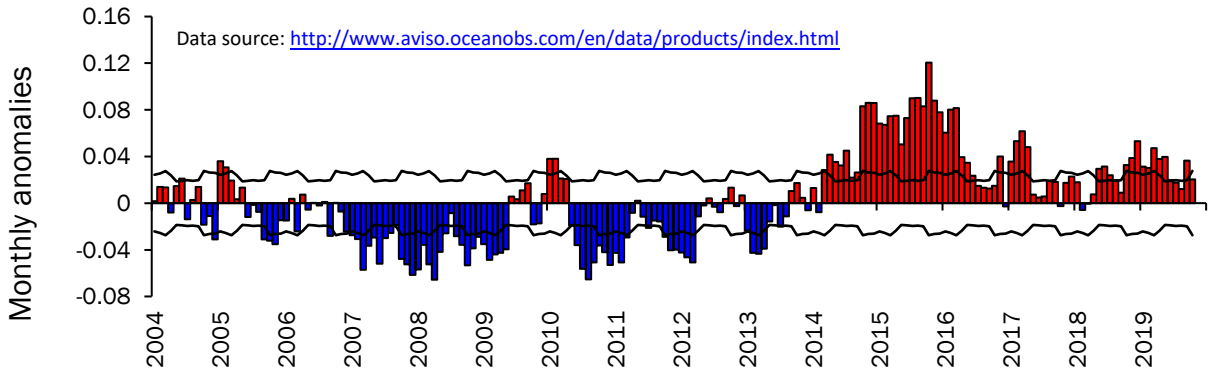

Figure 6. Monthly anomalies of sea surface heights, Aviso satellite, 2004–October 2019. Black lines represent ±99% confidence intervals around the long-term monthly means.

Upwelling

Local upwelling index derived from wind measurements from NOAA buoy 46013 in 2019 indicate mostly weak upwelling conditions (i.e. negative red bars) for the year (Figure 7). Strong local upwelling conditions were observed from late-2006 to early-2009, from 2012 to mid-2014, and in 2017-18. In contrast, NOAA upwelling indices (Pacific Fisheries Environmental Lab and Coastal Upwelling Transport Index) show strong upwelling conditions (i.e. positive blue bars) for most of 2019 (Figure 8) or a mix of upwelling conditions (Figure 9). These regional scale monthly NOAA upwelling indices are not capturing localized conditions detected by the buoys.

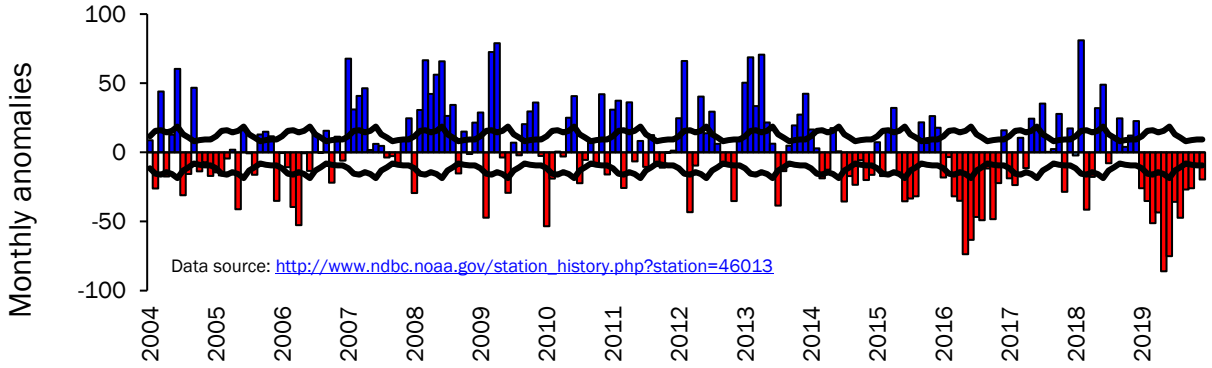

Figure 7. Monthly anomalies of upwelling indices, 2004–19 derived from wind at the Bodega buoy. Black lines represent ±99% confidence intervals around long-term monthly means. Red bars indicate weak upwelling/downwelling conditions, and blue bars indicate strong upwelling.

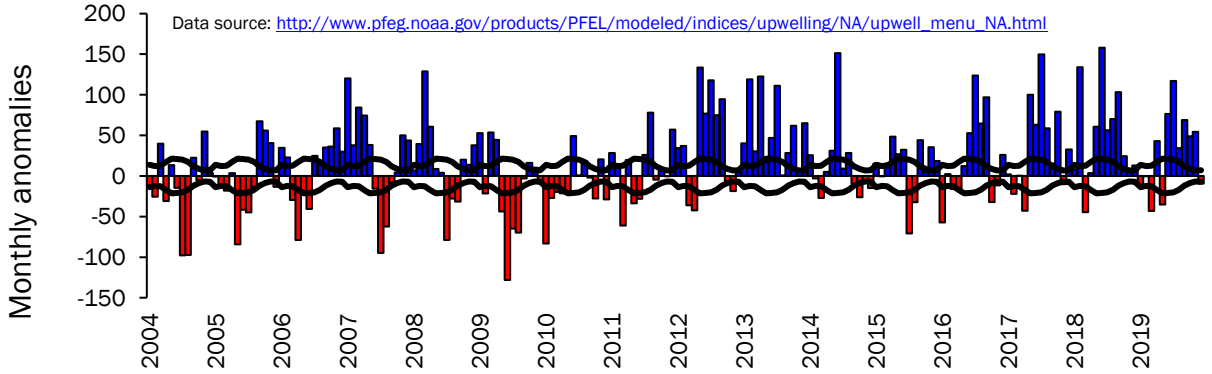

Figure 8. Monthly anomalies of upwelling indices, 2004–19 from Pacific Fisheries Environmental Lab. Black lines represent ±99% confidence intervals around long-term monthly means. Red bars indicate weak upwelling or downwelling conditions, and blue bars indicate upwelling.

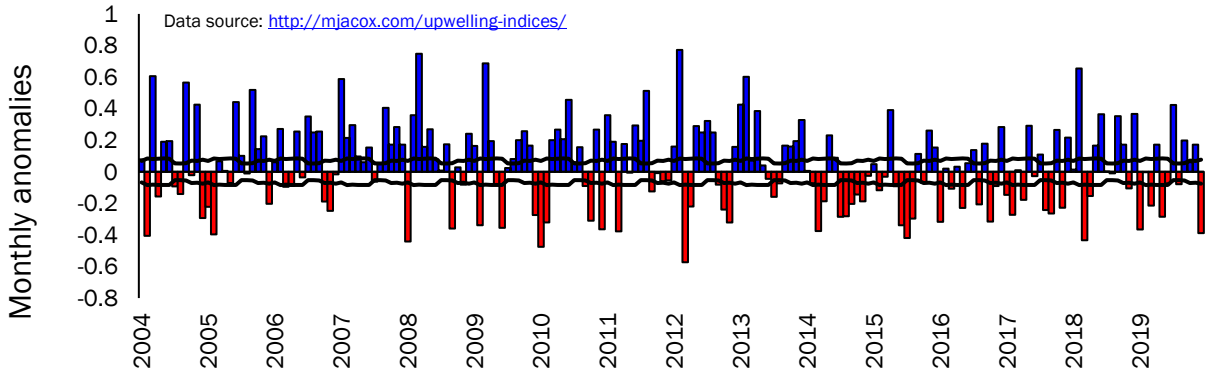

Figure 9. Monthly anomalies of the Coastal Upwelling Transport Index (CUTI), 2004–19. Black lines represent ±99% confidence intervals around long-term monthly means. Red bars indicate weak upwelling or downwelling conditions, and blue bars indicate upwelling.

Spring transition

Overview

The timing of the onset of upwelling can have significant effects on the marine ecosystem. The beginning of the upwelling season is known as the spring transition date, and earlier spring transition dates are linked to greater productivity in our regional marine ecosystem. If we consider March 31 (or March 30 in leap years) to be the average spring transition date, the earliest spring transition date in our time series was February 18 (in 2007, a cold water year), and the latest date was May 12 (in 1983, an El Niño year). See the NOAA Bodega Bay buoy data and NOAA PFEL Coastal Upwelling Indices sections in the Appendix for details on these data.

Spring transition

If we consider March 31st to be the long-term average spring transition date, the spring transition in 2019 was 10 days later (Figure 10). About half of the years since the start of the ACCESS program in 2004 (e.g. 2006-09, 2012-13, 2018) showed earlier transition dates (i.e. negative bars) and some years (e.g. 2005, 2010, 2016, 2019) had a late spring transition (i.e. positive bars; Figure 10). Local spring transition dates (calculated from Bodega Bay buoy data) show similar results as dates calculated from regional upwelling indices for most years; the transition date for 2019 was 57 days later than the long-term average (Figure 11). Late transition dates tend to be associated with El Niño events (e.g. 1983, 1998) and early dates with La Niña years (e.g. 2007).

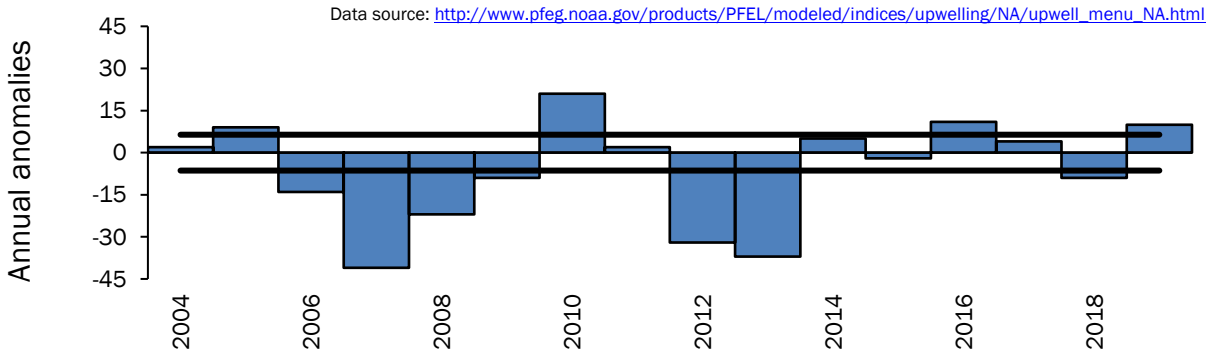

Figure 10. Anomalies of spring transition dates based on daily upwelling indices, 1972-2019. Black lines represent ±99% confidence intervals around 48-year mean. Negative bars indicate early transition dates, and positive bars indicate late transition dates.

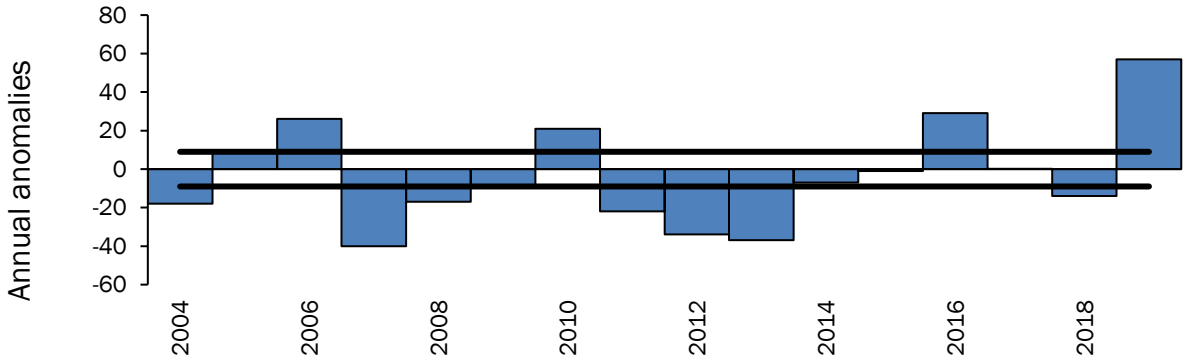

Figure 11. Anomalies of spring transition dates based on Bodega Bay buoy data, 1981-2019. Black lines represent ±99% confidence intervals around 39-year mean. Negative bars indicate early transition dates, and positive bars indicate late transition dates.

Sea Surface Temperature

Overview

Sea surface temperature (SST) is an indicator of the productivity of the ecosystem, as cold, nutrient rich water is brought to the surface during upwelling in early spring. The surface waters eventually warm up during relaxation events that follow upwelling, typically in late summer or early fall. We used NOAA weather buoy data and Southeast Farallon Island data for local observations, and satellite data (covering a 4 km^2 area) were used for a more regional perspective on SST. Each of these datasets shows an intra-annual pattern in SST for the entirety of their time series: a decline during upwelling (March-May), then increasing SSTs through September (which is the peak SST for the year), followed by another decline in the winter. See the NOAA Bodega Bay buoy data, Farallon Island sea surface temperature data, and sea surface temperature satellite data sections in the Appendix for details on these data.

Buoy SST

Local SSTs were warm (i.e. positive red bars) in the earlier months, then cool temperatures (i.e. negative blue bars) were observed in the latter part of 2019 (Figure 12). SSTs were

close to average values in the early months of 2004. In 2005 and 2006, anomalously warm SSTs were observed in the winter and spring months. In contrast, low SSTs (i.e. negative blue bars) were noted in most months of years 2007-13; short periods of average or warm waters (e.g. late months of 2008, early months of 2010) suggest local downwelling/relaxation events. The warm water event, known as the North Pacific heat wave, began in mid-2014, remained high through mid-2016, with overall warm ocean conditions thereafter.

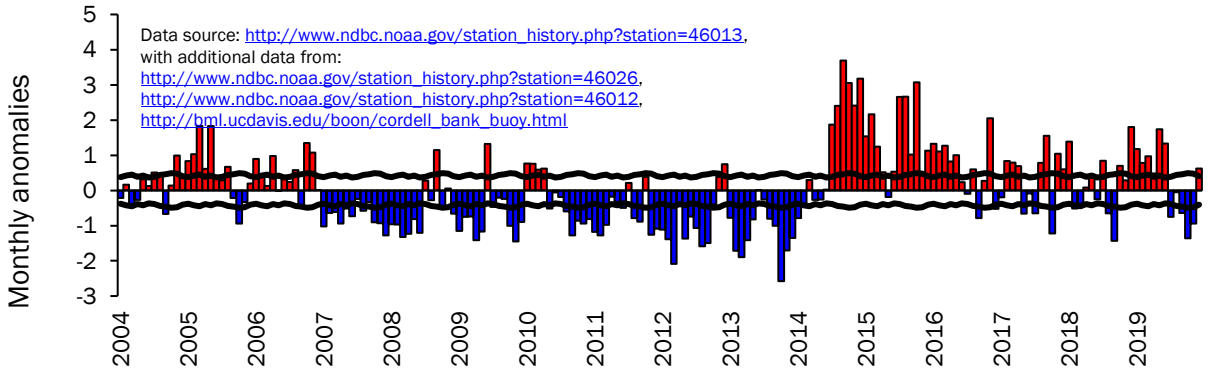

Figure 12. Monthly anomalies of SSTs, Bodega buoy, 2004-19. Black lines represent ±99% confidence intervals around the long-term monthly means.

Southeast Farallon Island SST

Data were only available through May 2019, yet this incomplete local time series shows warm (i.e., positive red bars) temperatures near Southeast Farallon Island (SEFI) for the first half of 2019 (Figure 13). Short upwelling events defined by cold waters were observed in 2004, but most values were closer to the long-term averages. Warm SSTs were observed throughout 2005-06 and 2014-19, although 2017-19 were cooler than 2014-16. Conversely, cold SSTs were observed throughout the early months of 2007-09, late 2010, and 2012-13. Cold temperatures appeared late (April and May) in 2010. SSTs in 2011 were normal to warm for most of the year.

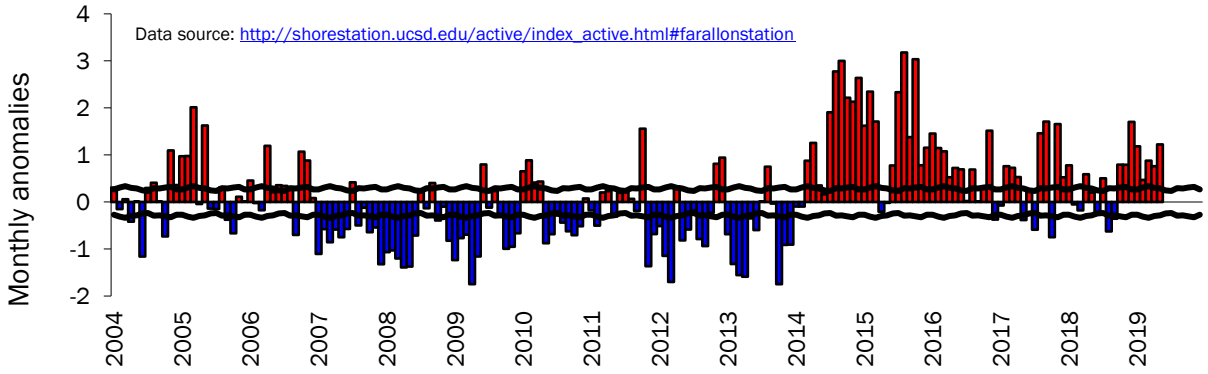

Figure 13. Monthly anomalies of SSTs, SEFI, 2004–May 2019. Black lines represent ±99% confidence intervals around the long-term monthly means.

Satellite SST

Satellite results shows warm (i.e., positive red bars) regional SSTs during most of 2014-19 (Figure 14). Temperatures in 2004 through mid-2005 were consistently warm; this differs

from the buoy and SEFI data, as these other data show periods of cold (i.e., negative blue bars), upwelled water at the surface. Similar to buoy and SEFI results, 2006 had warmer SSTs in the first half of 2006, and cold SSTs in the first half of years 2007-09. Warm waters in the early months and cold waters in the later months of 2010 are also consistent with other SST results. SSTs in 2011 were average, while 2012 and 2013 showed mostly cooler SSTs.

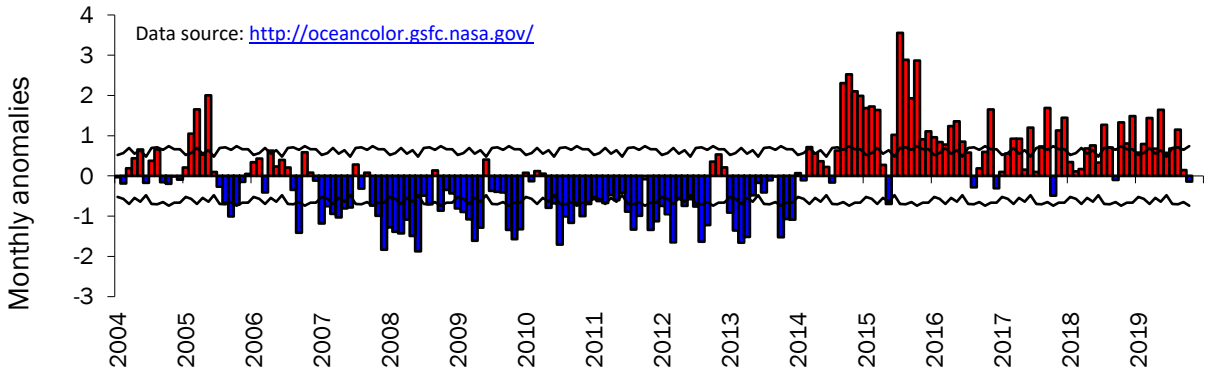

Figure 14. Monthly anomalies of SSTs, MODIS Aqua satellite, 2004–October 2019. Black lines represent ±99% confidence intervals around the long-term monthly means.

Sea surface salinity, ocean acidification, and hypoxia

Overview

Elevated sea surface salinity (SSS) values are also used as indicators of upwelling, as high sea surface salinities are generally associated with deeper nutrient-rich waters. Rising concentrations of atmospheric carbon dioxide (CO_2) have led to an increase in the amount of dissolved CO_2, which has decreased ocean pH (acidifying the water). An aragonite saturation state of 1 or above is favorable to shell building for calcifying organisms; < 1 is considered not favorable for shell building. ACCESS researchers have developed an algorithm using CTD data to quantify aragonite saturation levels. Hypoxia is defined as an incidence of low oxygen waters, particularly < 2 mg/L of dissolved oxygen. These low oxygen conditions are of concern for marine species, especially in benthic habitats where organisms may be less mobile or unable to move to areas with sufficient oxygen. With dissolved oxygen data collected during CTD casts during ACCESS cruises since 2010 (when the dissolved oxygen sensor was added to the CTD), ACCESS contributes to the understanding of when and where these hypoxic events occur. See the Farallon Islands sea surface salinity data and CTD recorder data sections in the Appendix for details on these data.

Southeast Farallon Island SSS

For 2019, only data through May were available at the time of this report; results show more saline (i.e. positive blue bars) present in Jan-Feb, followed by less saline waters (i.e. negative red bars) for Mar-May (Figure 15). Low salinity values were evident in 2004-06, indicating weak upwelling conditions. High salinity values were observed in early months of 2007-09, 2012-14, and 2018. Salinity values in 2010-11 and 2015-16 were average, indicating a lack of strong upwelling events in the early months of these years. The low salinity values in

2006 and 2017 may be the result of more freshwater outflow from the San Francisco Bay from wet winter conditions in these years.

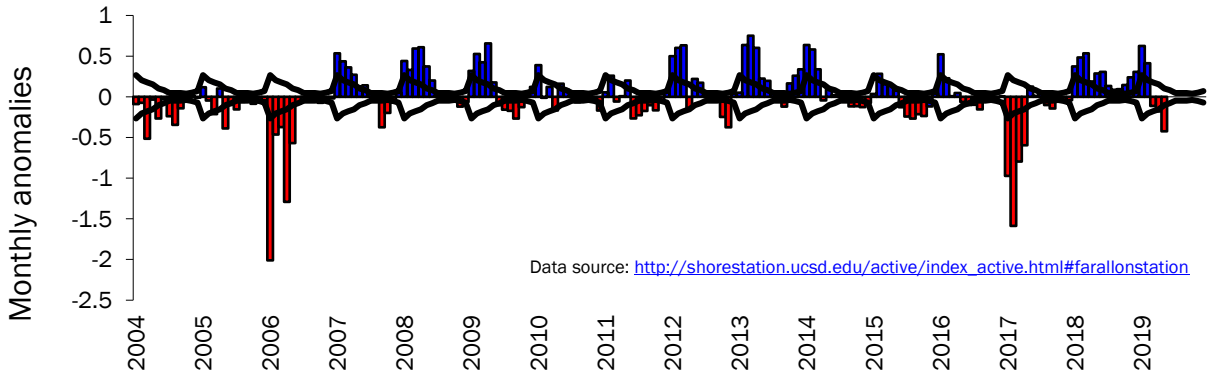

Figure 15. Monthly anomalies of sea surface salinity, SEFI, 2004–May 2019. Black lines represent ±99% confidence intervals around the long-term monthly means.

Aragonite saturation state

The local aragonite saturation state calculated using the relationship developed by Davis *et al*., 2018, at line 2, station W (west of Cordell Bank) during July cruises, showed low aragonite saturation states (< 1.0 Ω) throughout the water column in earlier years (e.g., 2010-11). In other years (2012-16), the aragonite saturation horizon (where Ω=1) varied from 30 m below the surface (e.g. 2014) to 60 m (e.g. 2018) to 90 m below the surface (e.g. 2012, 2016; Figure 16). In 2019, the horizon was around 100 m below the surface, with undersaturated waters observed throughout.

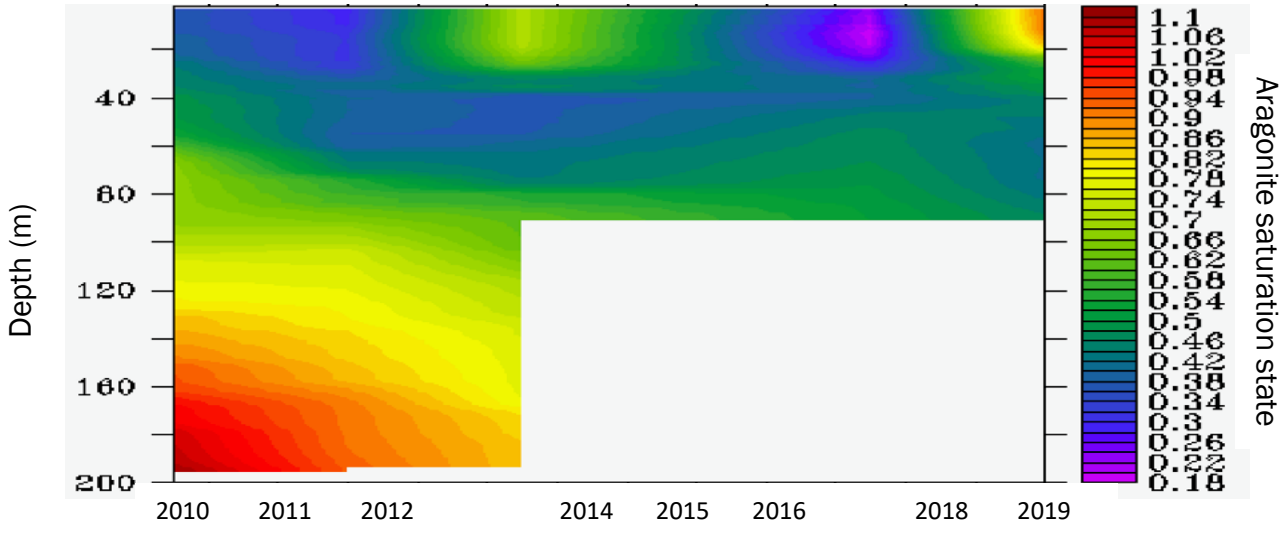

Figure 16. Aragonite saturation state measured to 200 m below the surface on July ACCESS cruises, line 2, station W, 2010-19. (Note: there were no CTD data from July cruises in 2013 and 2017.)

Dissolved oxygen

Local dissolved oxygen concentrations measured at line 2, station W (west of Cordell Bank) during July cruises showed hypoxic conditions (< 2 mg/L) at depth in 2011 (below 125 m),

and at shallower depths in 2011 (upper 40 m) and 2014 (80-90 m; Figure 7). Near-hypoxic conditions (< 5 mg/L) were noted ~60-90 m in most years (2010-12, 2015-16, 2018-19), and in shallower waters (~20 m) in 2014.

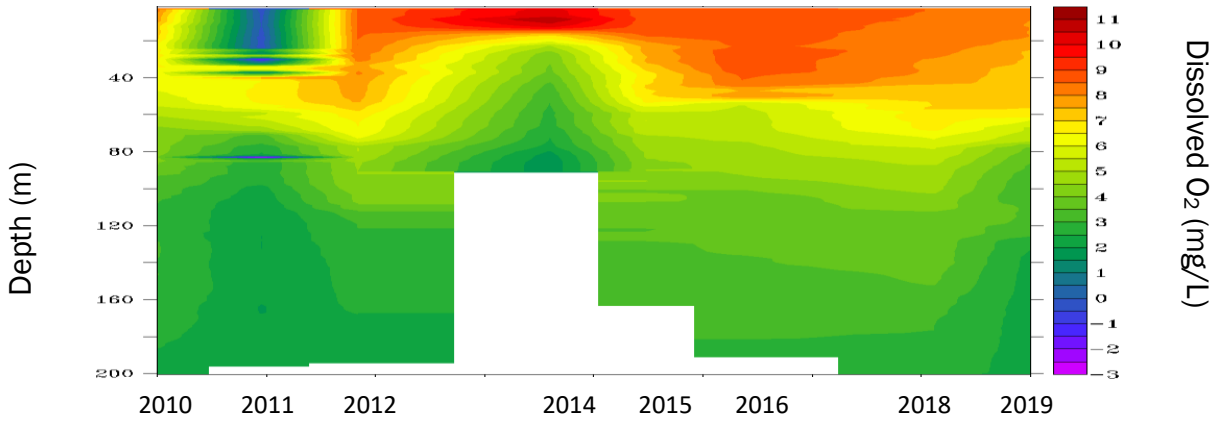

Figure 17. Dissolved oxygen concentrations measured to 200 m below the surface on July ACCESS cruises, line 2, station W, 2010 and 2012-19. (Note: there were no CTD data from July cruises in 2013 and 2017.)

Nutrients

Overview

Nutrients and sun light are critical for phytoplankton growth. Upwelling brings deep water rich in nutrients like nitrogen, phosphorus and silica to the surface layers of the ocean where phytoplankton have light from the sun for photosynthesis and the conditions needed for nutrient uptake. Phytoplankton need nitrate and phosphate for photosynthesis, while diatoms use silicate to build their cell walls. Nutrient concentrations can be used to track conditions conducive to primary production and the productivity of the regional marine ecosystem. See the surface water nutrients section in the Appendix for details on these data.

Surface water nutrient data

In 2019, local surface concentrations of nitrogen-based (NO_3+NO_2), phosphorus-based (PO_4), and silica-based (Si) nutrients in 2019 were low, with the exception of May when nitrates+nitrites and phosphate were slightly higher than average (Figure 18-20). Overall, this is a continuation of low nutrient conditions observed since 2013. Other warm-water events (e.g. 2005-06, mid-2009) also showed reduced nutrient concentrations, while higher concentrations were observed in cold-water regimes (e.g. 2007-08, early 2009).

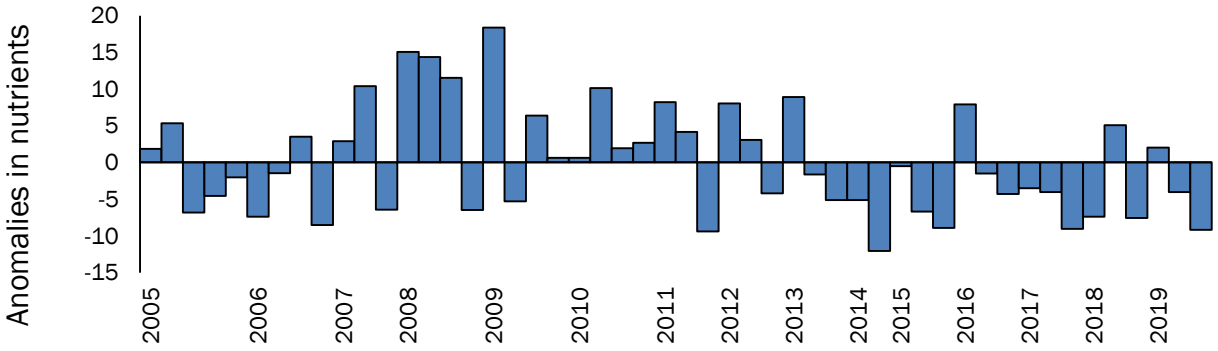

Figure 18. Monthly anomalies in average surface concentrations of nitrates (NO_3) and nitrites (NO_2) in sea surface water from ACCESS cruises, 2005-19.

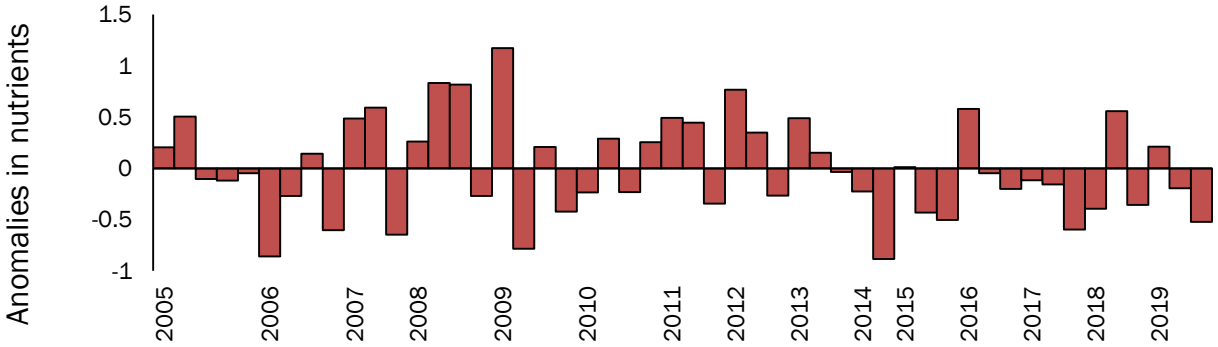

Figure 19. Monthly anomalies in average surface concentrations of phosphates (PO_4) in sea surface water from ACCESS cruises, 2005-19.

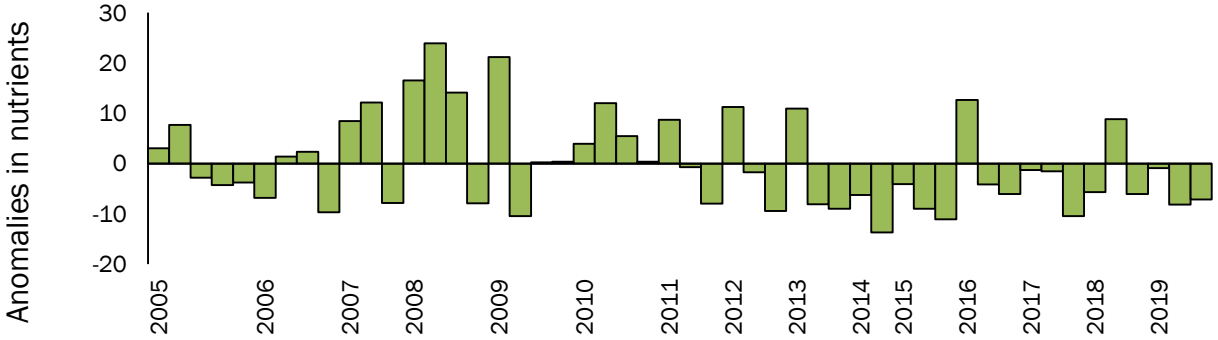

Figure 20. Monthly anomalies in average surface concentrations of silicates (Si) in sea surface water from ACCESS cruises, 2005-19.

Biological Ocean Climate Indicators

Chlorophyll a and phytoplankton composition

Overview

Concentrations of chlorophyll a can provide information on the amount of phytoplankton in surface waters. The timing of peak phytoplankton abundance could also have effects on marine ecosystem productivity. Satellite data provide us with phytoplankton abundance estimates; long-term monthly means in abundance show increasing phytoplankton abundance in March-May, a slight decline through September, then a peak in October. Phytoplankton collected within and adjacent to the sanctuaries was analyzed by the California Department of Health to evaluate Harmful Algal Bloom (HAB) species, which also helps us understand the phytoplankton community composition. Composition of the phytoplankton community can provide insight into how productive an ecosystem might be. For instance, an increase in the abundance of dinoflagellates (a small organism) could signify poor ocean conditions, whereas a greater abundance of diatoms (a larger organism) could indicate more productive ocean waters. See chlorophyll a satellite data and phytoplankton species composition data sections in the Appendix for details on these data.

Satellite Chlorophyll a

Regional phytoplankton blooms (i.e. positive anomalies) were observed in May-June of 2019 (Figure 21). Although typically upwelling is associated with productivity, overall, ocean color data shows that phytoplankton blooms are more common during weak upwelling years as indicated by positive anomalies in 2004-06 and 2013-16. Negative anomalies generally correspond to intense upwelling years from 2007-12, when relaxation and stratification are reduced. Blooms are known to occur after the seasonal thermocline is established, so the peak chlorophyll a concentrations in later months (fall and winter) of 2005 and 2006 could be explained by the delayed upwelling in those years. Strong upwelling and a lack of relaxation could explain the average to low phytoplankton abundance in 2007-12. Blooms appeared more frequently in 2011 but were relatively low.

Figure 21. Monthly anomalies of chlorophyll a, MODIS Aqua satellite, 2004–Oct 2019. Black lines represent ±99% confidence intervals around the long-term monthly means.

California Department of Public Health data

The local phytoplankton community sampled in offshore stations for 2019 was largely dominated by diatoms in Mar-Jun, and then switched to dinoflagellates in the fall (Figure 22), which is indicative of lower than average ecosystem productivity. Large percentages of diatoms have been observed in recent years (2010-18), which is typically indicative of good ecosystem productivity. Sampling locations have varied through time (i.e., more southern stations sampled in 2004-09, more northern stations sampled in 2014-18), stations in the core area sampled since 2004 show this trend of increasing diatoms through time. Some years (e.g. 2006, 2007, 2009, 2011, 2018) showed an increase in percent composition of dinoflagellates from spring/summer to fall/winter, while other years (e.g. 2010, 2012-13, 2017) showed a decline in percent composition of dinoflagellates in the fall/winter. Dinoflagellates are most associated with warm, less turbulent waters later in the year (when diatoms sink and become scarce in surface waters) and are responsible for HABs common in the fall months; the exception to dinoflagellates causing HABs are diatoms in the genus *Pseudo-nitzschia*, which are responsible for domoic acid events. Unlike most years, dinoflagellates were relatively more abundant than diatoms in the spring/summer of 2008.

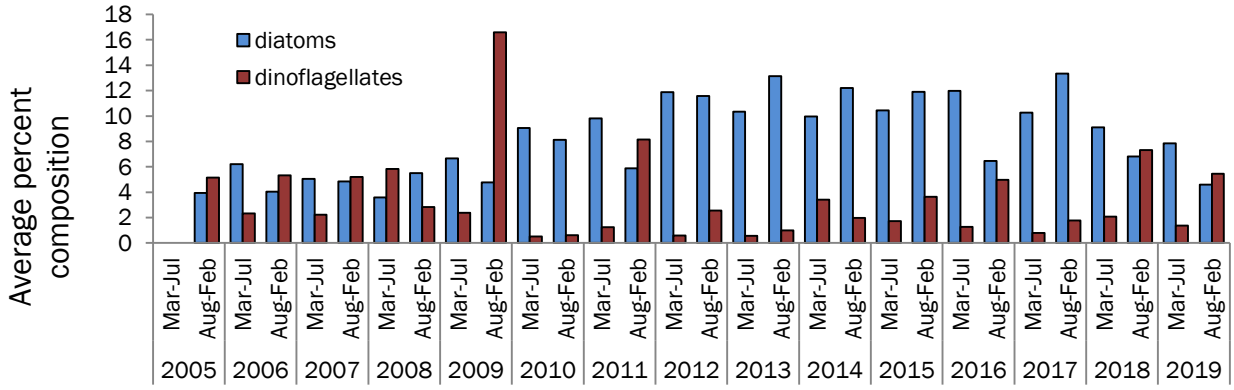

Figure 22. Average relative composition of diatoms and dinoflagellates in offshore samples, 2005-19.

Zooplankton composition

Overview

Information on the abundance and species composition of zooplankton are also indicators of the productivity of an ecosystem. For example, analysis of ACCESS data shows an overabundance of gelatinous species can signify poor productivity, and a highly productive ecosystem may have high abundances of euphausiids, which are important prey for fish, seabirds, and marine mammals. See the zooplankton data section in the Appendix for details on these data.

Overall relative composition

While 2016-19 ACCESS hoop net data are not yet available, we can see variability in the local zooplankton abundance and composition in years 2004-15 (Figure 23). Anecdotal observations of zooplankton samples taken during 2014-15 ACCESS cruises appeared to be dominated by gelatinous zooplankton; low abundances of small euphausiids reappeared in

summer 2015 and larger densities of larger euphausiids were present in fall 2015. From September 2004 through October 2006, the overall average abundance of zooplankton was greatly reduced and never reached over 30 individuals per cubic meter of water sampled. The trend changed in 2007, when overall zooplankton abundance increased dramatically, and this overall increase in zooplankton abundance is sustained for most surveys in 2007 and 2008. This is mainly attributed to increases in euphausiid and copepod abundance. The first half of 2009 shows high zooplankton abundance (especially euphausiids and copepods), followed by a return to low zooplankton densities. Results from 2010-11 show increasing zooplankton abundances, with a significant increase in euphausiids. A decline in zooplankton abundance occurred in early 2012 and increased again through June 2014. While euphausiid abundance was down in 2014, tunicates (represented in the "Other" category) were very plentiful. While we do not have samples from each month of the year, our results show a peak in June in some years (e.g. 2007-09), while the latter years (e.g. 2010-14) show a peak in September.

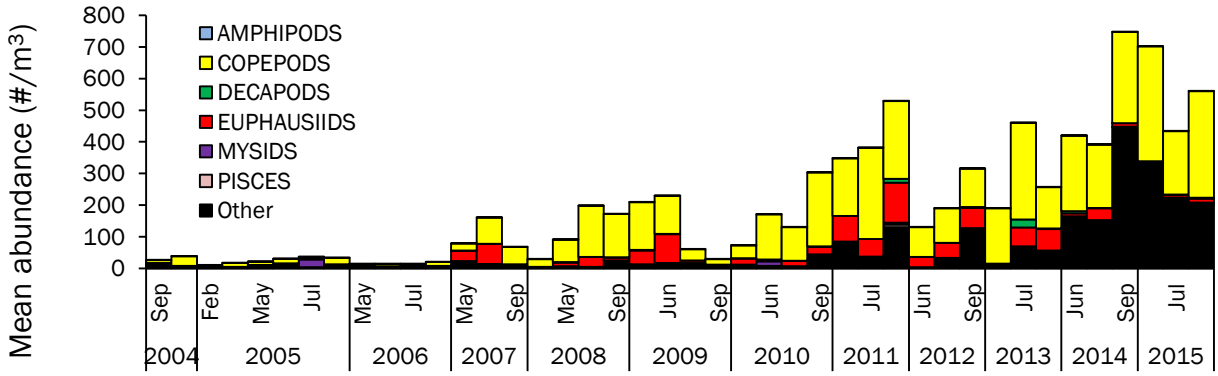

Figure 23. Zooplankton composition in the upper 50 m of the water column determined from hoop net samples, 2004-15. NOTE: Euphausiid abundances include all life stages except eggs.

Overall community analysis

We looked for similarities between sampled years based on the ACCESS hoop net zooplankton species composition data by performing a non-metric multi-dimensional scaling analysis for samples collected in the spring and summer months (Apr-Jul; Figure 24). In general, there appear to be two main groups that cluster together: years 2004-06 (warm regime years), and years 2007-13 (cold regime years). Conditions in mid-2009 changed from cold waters to warm waters, which revealed a change in the zooplankton community (Fontana *et al*., 2016), and this could be one reason for the departure of some of these samples from the others in the 2007-12 group. Results that we have for 2014-15 appear just outside of the boundaries of these two groups; these years represent the North Pacific heatwave and an increased abundance of tunicates (mainly doliolids).

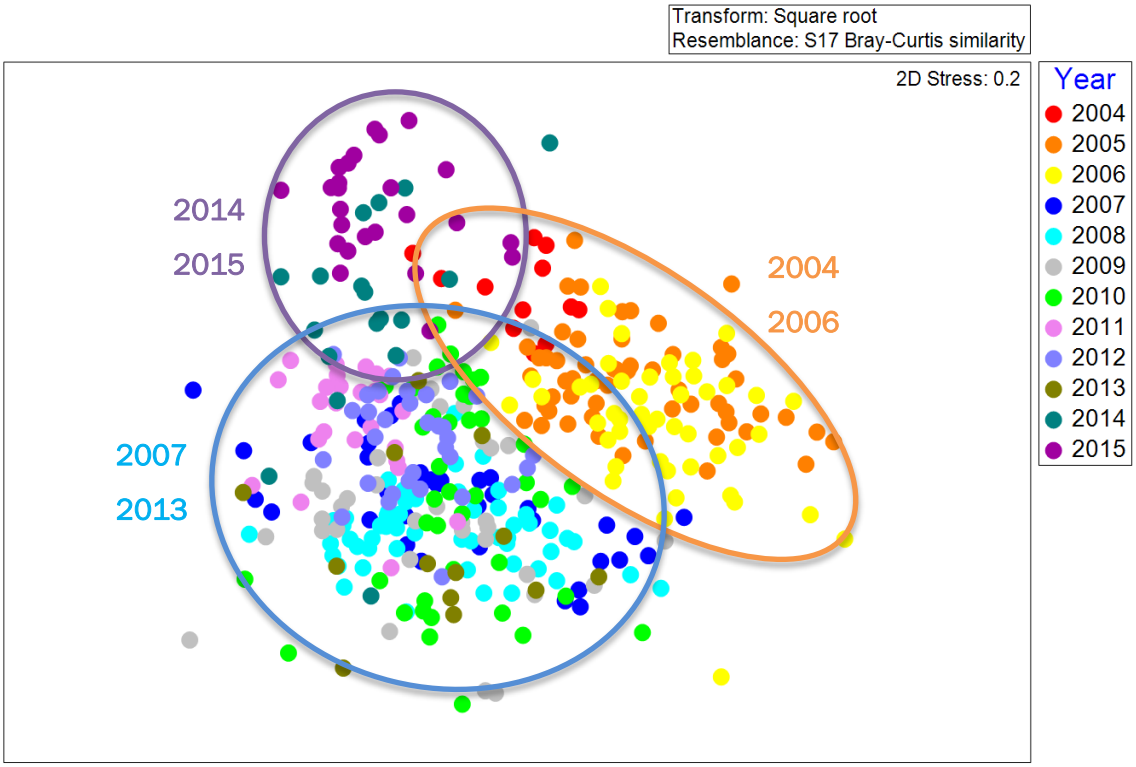

Figure 24. Non-metric multi-dimensional scaling analysis of zooplankton, April-July samples, 2004–15.

Copepods

Overview

The ACCESS study area is predominantly within an area we call the "transition zone." Copepods are mid-trophic level organisms, and they are the most abundant and diverse zooplankton taxa, constituting the largest source of protein in the marine environment. Copepod communities change in response to changing oceanographic conditions, and the presence and absence of key species can indicate these changes. Copepods that are common to northern latitudes (called boreal species) become more abundant in colder, productive ocean waters (roughly north of 40°N). Transition zone copepods species are common to the temperate latitudes (20-40°N), yet they can become more abundant in colder waters and less abundant in poor ocean conditions. Equatorial species (i.e., species from tropical or subtropical regions, ~10-20°N) can be found during warm water intrusions into our study area (e.g., El Niño events). See the zooplankton data section in the Appendix for details on these data.

Relative composition

While we do not yet have ACCESS hoop net data for all years, the results we do have indicate changes in the local copepod species composition, the most notable in the boreal species (Figure 25). In general, these species were in reduced abundances during warm water regimes (e.g. 2004-06 and 2015) and higher abundances during cold water regimes (e.g. 2007-early 2009, 2010 through early 2014). While we do not have samples from each

month of the year, our results for boreal copepods generally show peak abundance in May-June, and declining densities in fall, but this varies with ocean conditions (e.g. 2009, 2010). Species common to mid-latitude areas were in relatively low abundances throughout the time series, with increased abundances in the latter years (2011-15; Figure 26). Our within-year results varied greatly, with peak abundances in June for some years (e.g. 2007, 2009, 2015) and September/October for others (e.g. 2005-06, 2010-14). Equatorial copepods remained in low abundances throughout the twelve years, except for high densities in 2007 and slight increases in abundance in 2011, late 2014, and 2015 (Figure 27). Peak abundances are typically during September cruises (e.g. 2007-09, 2011-14).

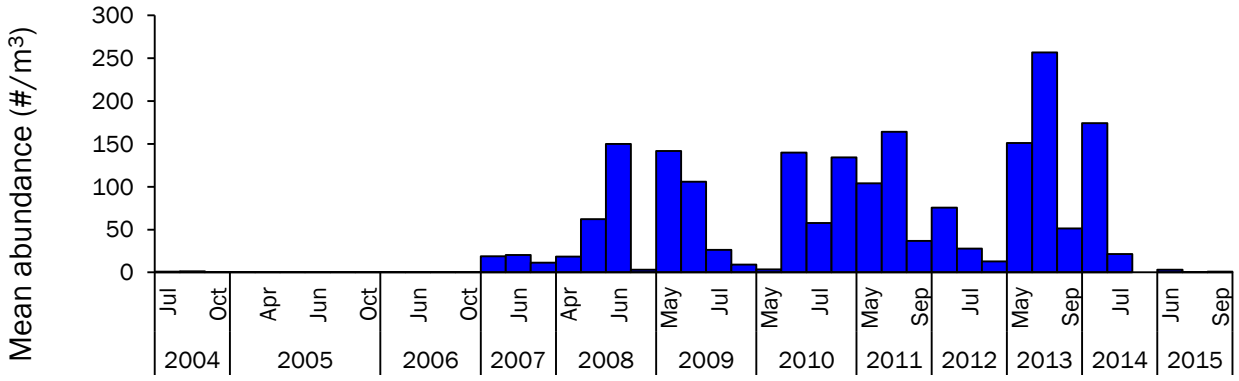

Figure 25. Average abundances of boreal copepod species, 2004-15.

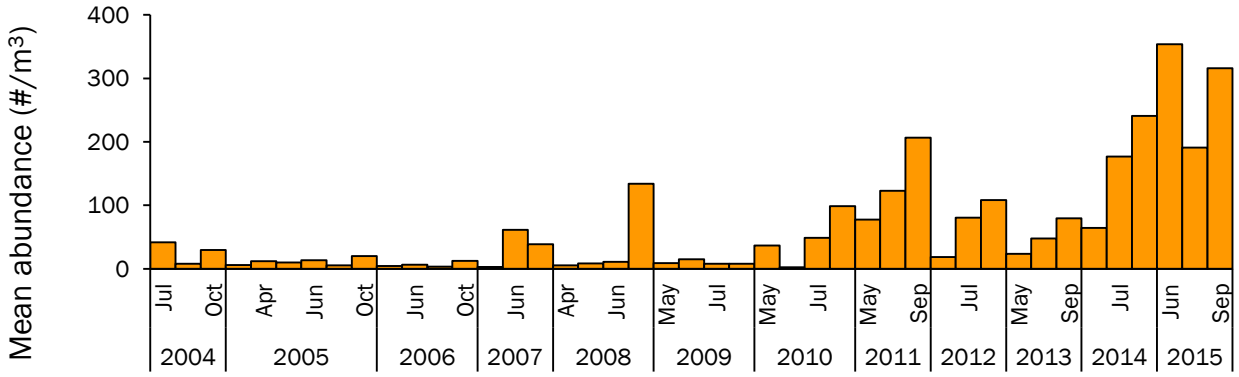

Figure 26. Average abundances of transition zone copepod species, 2004-15.

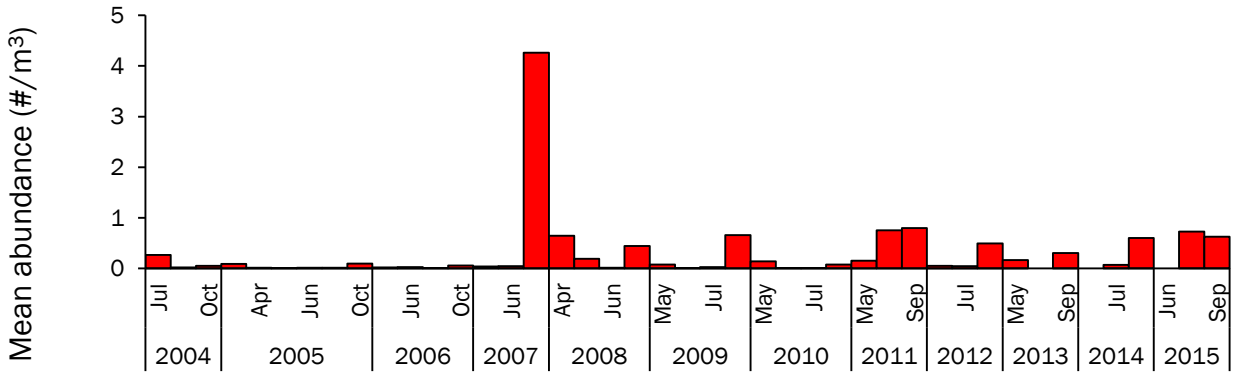

Figure 27. Average abundances of equatorial copepod species, 2004-15.

Pteropods

Overview

Pteropods are pelagic marine gastropods and are commonly known as sea butterflies. There are two orders of these mid-trophic level organisms: Thecosomata and Gymnosomata; the former contains a shell while the latter does not. One species belonging in the order Thecosomata, *Limacina helicina*, has been used to study the effects of ocean acidification. This species' calcium carbonate shell is sensitive to dissolution in acidic conditions, and shell thickness can be measured on this species to assess impacts of ocean acidification and its effects on the marine environment. *L. helicina* has been classified as a key indicator species of ocean acidification for our study area (Duncan *et al*., 2013). See the zooplankton data section in the Appendix for details on these data.

Abundance

We do not yet have the ACCESS hoop net results from 2016-18. However, results we have so far reveal very low abundances of *L. helicina* in our study area during the first two years of our study (Figure 28). Increases were first noted in June 2006 (which may have coincided with the beginning of the delayed upwelling in that year). Abundances have remained at low levels, with increased abundances noted in 2010-12. A decline in pteropod abundance was observed in 2013-15, with no *L. helicina* observed in 2014. We are currently investigating the temporal and spatial patterns in *L. helicina*, as well as the oceanographic conditions related to higher abundances of this species.

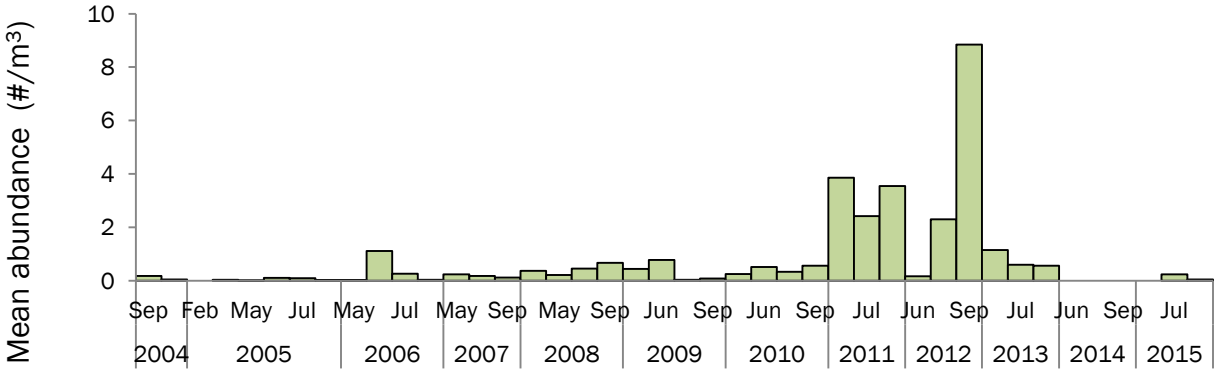

Figure 28. Average abundance of the pteropod Limacina helicina, 2004-15.

Euphausiids

Overview

Euphausiids (commonly known as krill) are important mid-trophic level organisms. They feed mainly on phytoplankton and are prey for many marine top predators (e.g., salmon, seabirds, and whales). There are two main species found in our study area: *Euphausia pacifica* and *Thysanoessa spinifera*, the former being more abundant than the latter. Adult and immature stages of these species are known to be the primary prey items of the Cassin's auklet, a zooplanktivorous seabird species breeding on the Farallon Islands, and for blue and humpback whales. When euphausiids are available, how abundant they are, and the size classes available (i.e. zoea, juveniles, adults) are important to the marine ecosystem. See the zooplankton data and hydroacoustics data sections in the Appendix for details on these data.

Abundance

Acoustic biomass results from ACCESS cruises are not yet available for 2019. Results for 2018 show the highest local euphausiid abundance in June, then a sharp decline in July and September (Figure 29). Abundance of euphausiids down to 200 m below the surface were lower in the first 5 years of monitoring (2004-08, with early 2006 as the exception) with seasonal peaks in spring/summer, followed by increased abundance in 2009-11. Euphausiid abundance appeared to wane in 2012-16, with periods of heightened biomass (e.g. June 2015, July 2016), then a rise in abundance in 2017. June 2018 was the highest krill abundance in the 15-year time series. It is worth noting that these peaks and dips in abundance do not necessarily align with warm or cold conditions. While we do not have samples from each month of the year, our results indicate annual peaks in euphausiid abundance appeared to shift from mostly May or June cruises (2004-09, 2014-15, 2018) to July cruises (2010-13, 2016-17). The large 2006 densities are likely an artifact due to salps and other gelatinous zooplankton that were abundant that year, as these species can confound acoustic results.

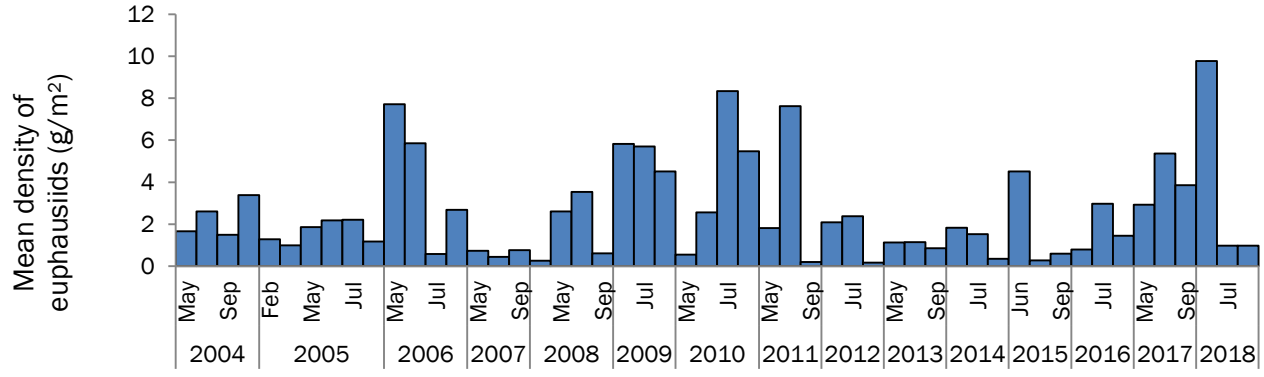

Figure 29. Acoustic biomass of euphausiids down to 200 m, 2004-18.

Euphausiid age classes

Adult *E. pacifica* in ACCESS Tucker trawl samples (i.e., sampling down to 200 m) comprised ~80% by wet weight of May 2019 samples but declined to ~60% in September (Figure 30). Adult euphausiids were more abundant during the cold, productive conditions of 2007-08,

as well as average conditions in 2010-11, while younger stages dominated during the warm, less productive conditions observed of 2005-06, and later months of 2009, 2012, 2014-15, and 2017. Adults were abundant for most of 2010-13, although percentages appear to be declining through time, with fall cruises (Sep) usually show higher percentages of the younger life stages.

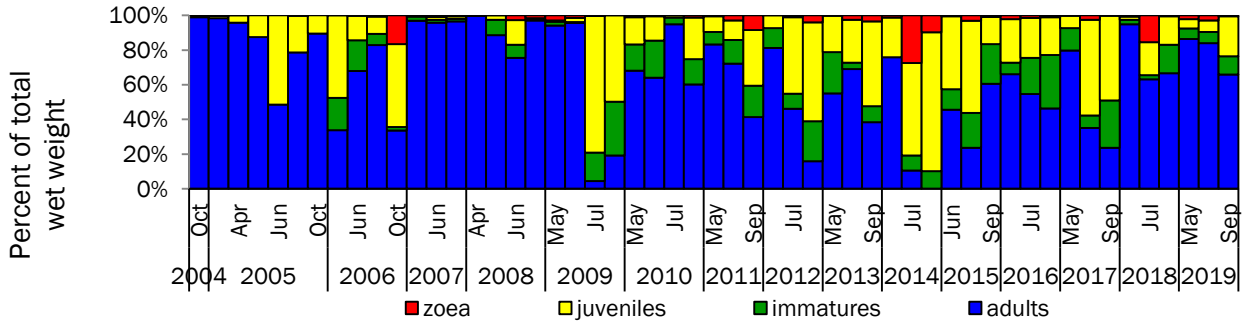

Figure 30. Percent composition of Euphausia pacifica age classes, 2004-19.

Variability in adult euphausiid sizes

Local adult *E. pacifica* caught in ACCESS Tucker trawls vary in size depending on annual ocean conditions (Figure 31). When we combine results from the cold water years (e.g. 2007-13), the length frequency distribution peaks at 13 mm and 20 mm. Warm water years (e.g. 2005-06, 2014-16) show only one peak at 13 mm. Since the marine heatwave, results from 2017 looked similar to warm water years (peak at 13 mm), while 2018 and 2019 samples had larger krill (peaks at 16 mm). Overall, cold conditions result in larger adult euphausiids compared to warm conditions.

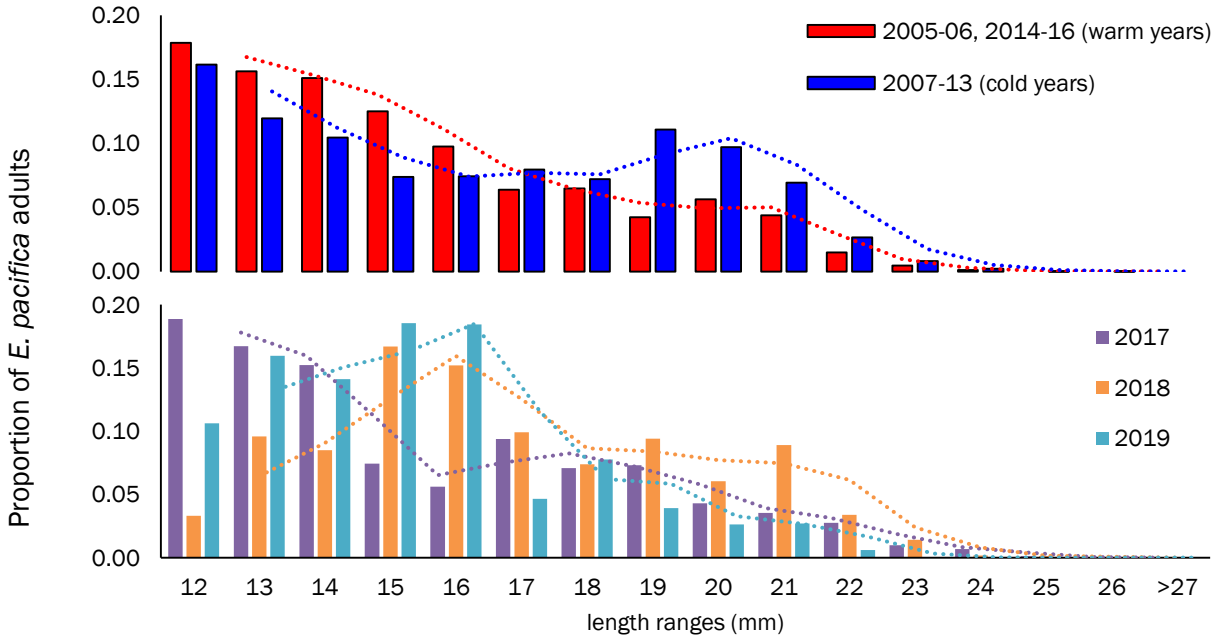

Figure 31. Length frequency distributions for adult Euphausia pacifica caught in Tucker trawls during spring/summer (May-July), warm/cold regimes (2005-16, top) and post-marine heatwave years (2017-19, bottom).

Birds

Overview

Seabirds are top marine predators that feed on a variety of marine organisms. Some species breed within our study area, while other species migrate great distances to forage within the study area and throughout the central California Current. The abundances and distributions of marine birds have been linked to bathymetric and hydrographic features that aggregate prey; many seabirds live in or travel to the central California Current because of the highly-productive waters common to our study area. Seabird reproductive success has been linked to the abundance of high-lipid prey near their breeding colonies (Frederickson *et al*. 2013, Dahdul & Horn 2003, Becker *et al.* 2007). See the bird observations and Southeast Farallon Island seabird data sections in the Appendix for details on these data.

Relative composition

There were a total of 56 species of seabirds identified during at-sea cruises (Table 2).

Table 2. Seabird species and average densities per cruise, 2004-19.

Common Name	Average density (#/km² of surveyed area)	Common Name	Average density (#/km² of surveyed area)
common murre	19.4117	pomarine jaeger	0.0071
sooty shearwater	10.7055	surf scoter	0.0039
Cassin's auklet	8.6573	unidentified auklet	0.0037
pink-footed shearwater	1.1965	South Polar skua	0.0027
western gull	1.1802	double-crested cormorant	0.0027
Brandt's cormorant	0.8501	flesh-footed shearwater	0.0027
rhinoceros auklet	0.7681	parasitic jaeger	0.0023
red-necked phalarope	0.6766	glaucous-winged gull	0.0022
ashy storm-petrel	0.4329	ancient murrelet	0.0021
unidentified phalarope	0.4328	unidentified storm-petrel	0.0018
fork-tailed storm-petrel	0.3138	common loon	0.0017
California gull	0.3035	elegant tern	0.0015
northern fulmar	0.2788	Laysan albatross	0.0014
black-footed albatross	0.2090	Canada goose	0.0008
pigeon guillemot	0.2043	peregrine falcon	0.0008
red phalarope	0.1669	unidentified duck	0.0008
unidentified gull	0.0832	Thayer's gull	0.0008
Buller's shearwater	0.0825	unidentified loon	0.0008
Sabine's gull	0.0441	mottled petrel	0.0007
Heermann's gull	0.0415	red-throated loon	0.0007
Arctic tern	0.0369	Wilson's storm-petrel	0.0007
unidentified shearwater	0.0360	black scoter	0.0007
pelagic cormorant	0.0296	herring gull	0.0004
tufted puffin	0.0291	unidentified murrelet	0.0003
black-legged kittiwake	0.0269	western grebe	<0.0001
black storm-petrel	0.0180	Caspian tern	<0.0001
brown pelican	0.0176	Clark's grebe	<0.0001
Pacific loon	0.0112	mew gull	<0.0001
unidentified alcid	0.0101	western/Clark's grebe	<0.0001
Bonaparte's gull	0.0096	marbled murrelet	<0.0001
Scripps's murrelet[1]	0.0087	ring-billed gull	<0.0001
unidentified dark shearwater	0.0085	black-vented shearwater	<0.0001
short-tailed shearwater	0.0079	unidentified bird	<0.0001

[1] This species includes Xantus's murrelet, Scripps's murrelet, and Scripps's/Guadalupe not distinguished.

When looking at the ten most abundant seabird species, six of these are known to breed on SEFI or other areas within the central California Current. Sooty and pink-footed shearwaters

overwinter in the study area, and red-necked phalaropes can be found here as they make their way from their Arctic breeding grounds to tropical waters for the non-breeding period.

The next few sections will concentrate on the information available on some of these abundant species, particularly three species that breed on SEFI and forage in the ACCESS study area: Cassin's auklet, common murre, and Brandt's cormorant. These species are identified as climate change indicator species (Duncan *et al*. 2013).

Cassin's auklet

Brief species account

The Cassin's auklet is a small burrowing seabird that breeds on the Farallon Islands. This is a zooplanktivorous species, with the majority of their diet consisting of euphausiids.

Abundance

In 2019, densities of Cassin's auklets were very low, with peak density (4 auklets/km^2) observed in May (Figure 32). The highest abundance of Cassin's auklets in the time series was found in May 2004 (106 auklets/km^2). After this, less than half this peak density was observed in any cruise. In general, counts were higher during the breeding season (Mar-Aug). The lowest number of auklets was found in 2006, the year with delayed and weak upwelling conditions. Numbers rebounded to some degree in 2009-17. Intra-annual results track the euphausiid acoustic results, with peak numbers occurring during June for most years through 2008, then peak auklet counts shifted to July for the remaining years.

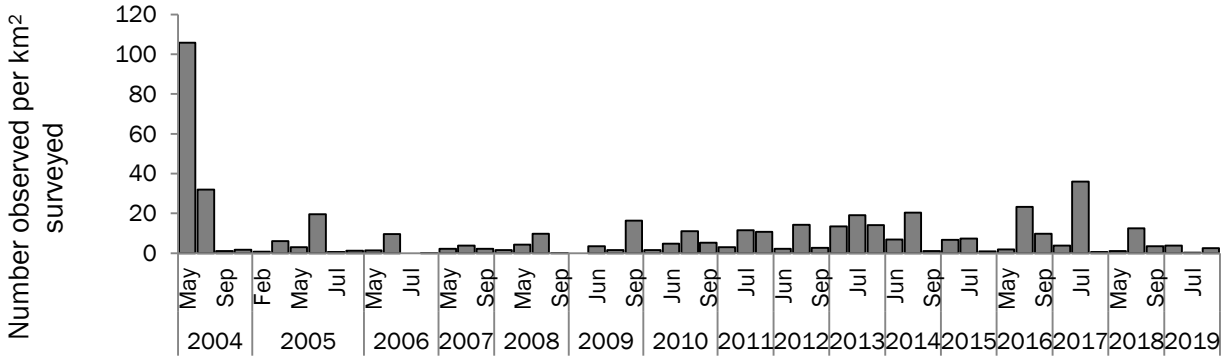

Figure 32. Abundances of Cassin's auklets observed during each cruise, 2004-19.

Distribution

Cassin's auklets were observed primarily over Cordell Bank in May 2019 (Figure 33). Cassin's auklets are raising chicks during the months of May and June, which is why they were found close to SEFI in some years (e.g., 2015 (not shown here), 2016-18). While not shown here, poor upwelling years (e.g. 2005-06) were characterized by smaller auklet flocks, and they ventured farther north and nearshore. Improved ocean conditions returned in 2007, and auklets were observed over Cordell Bank, along the shelf break and closer to SEFI, but not in the large flocks noted in 2004.

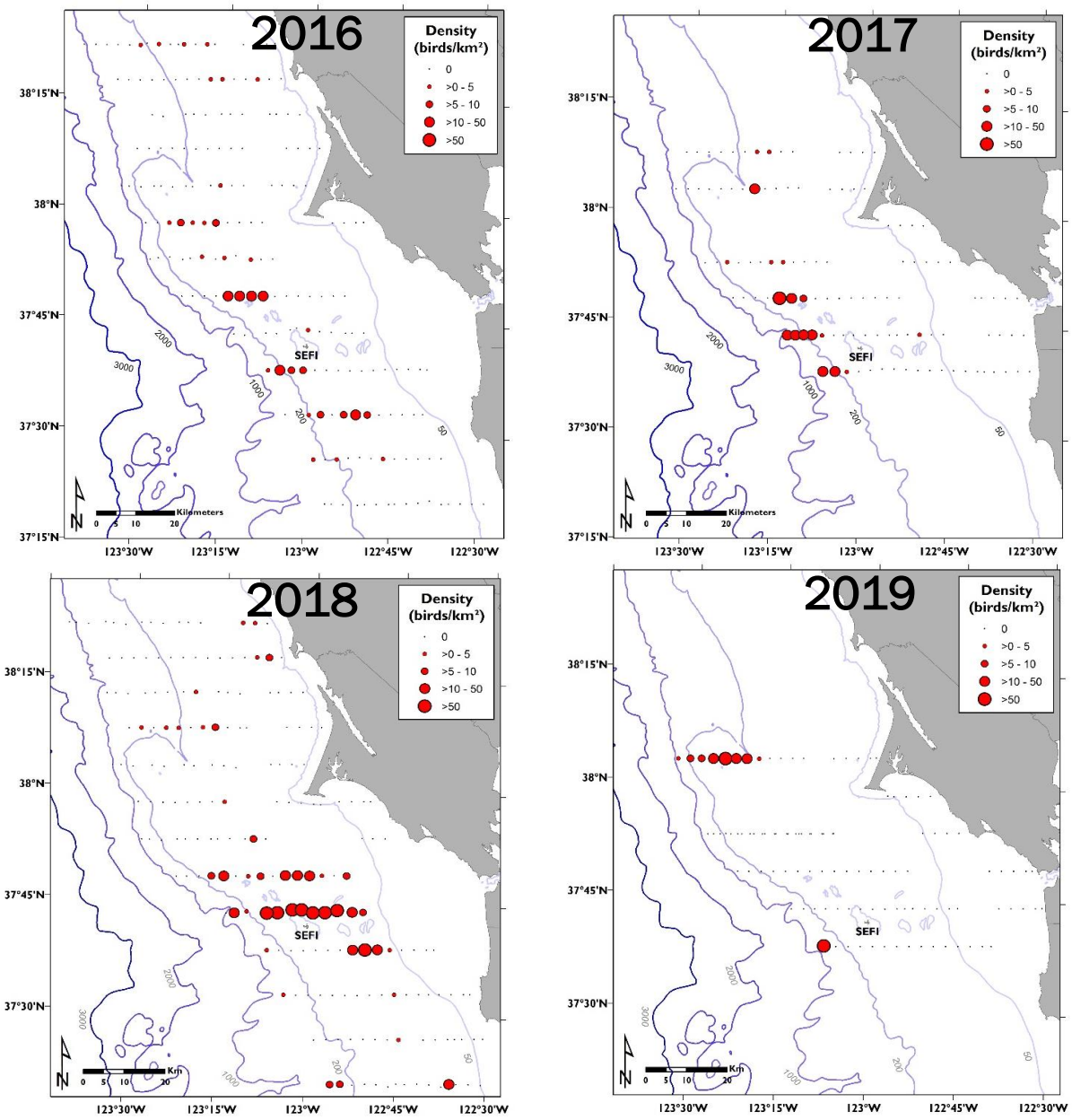

Figure 33. Cassin's auklet distributions during May or June 2016-19.
NOTE: July 2018 is shown here, as the May survey only covered a small area.

Timing of breeding

The Cassin's auklet median egg lay date for 2019 was 12 days later than the 48-year average on SEFI (Figure 34). Anomalously late lay dates correspond to El Niño events (e.g., 1982, 1992, 1998), when ocean conditions were poor. Since 2004, lay dates for Cassin's auklets have been average or earlier than the long-term average, with only 2005 (i.e., a poor ocean condition year) being noticeably later. There is a slight trend towards later lay dates through the time series, but this is not significant.

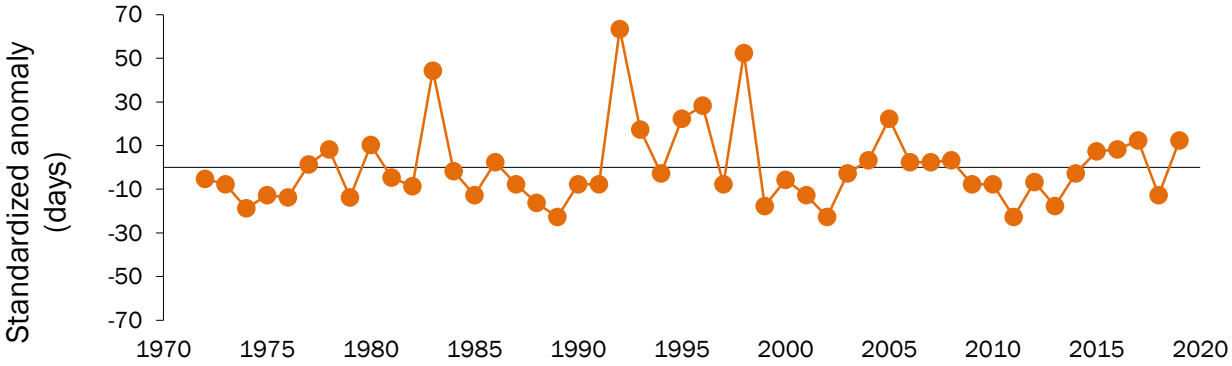

Figure 34. Cassin's auklet annual median egg lay dates on SEFI, 1972-2019.

Breeding success

Breeding success for the Cassin's auklet on SEFI was anomalously low in 2019, plotting below the 80% confidence interval for the 49-year mean (Figure 35). The anomalously low productivity years have occurred during El Niño years (e.g., 1983, 1992) and generally correlate with years of later egg laying (Figure 34); years 2005 and 2006 are exceptions, as these were not El Niño years and lay dates were near the average, but they were the worst productivity years on record. Surprisingly, the warm water conditions in 2014-15 did not translate to reduced productivity for this species. Conversely, earlier lay dates (e.g., 2009-13; Figure 34) were linked to better productivity, indicating that an earlier start to breeding can lead to higher breeding success.

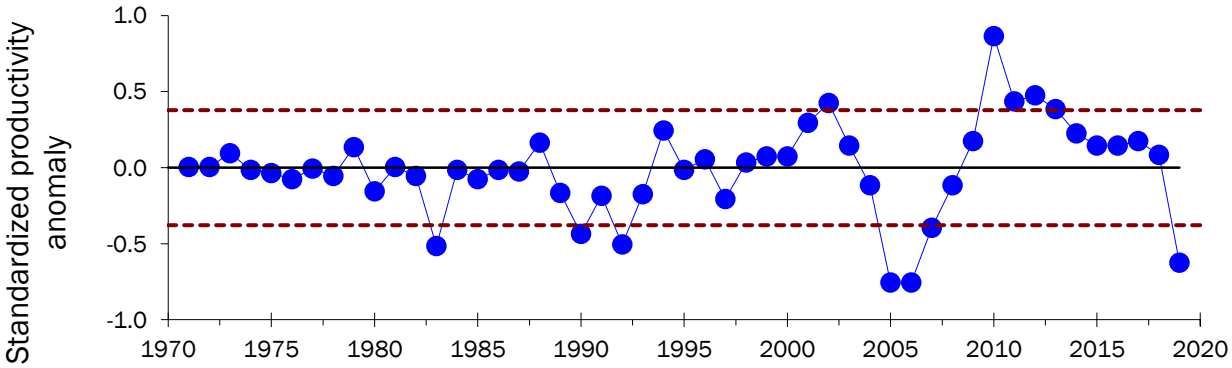

Figure 35. Cassin's auklet breeding success anomalies on SEFI, 1971-2019. Solid black line represents 49-year mean, and dotted red lines represent ±80% confidence intervals.

Diet

We do not yet have results for 2019. In 2018, Cassin's auklets consumed mostly euphausiids, and this was the case for the 38-year diet time series for Cassin's auklets (Figure 36). The diet in 2005-06 deviate greatly from the other years, as mysids (shrimp-like marine invertebrates) comprised the entire diet of the few diet samples collected in those years. This also led to breeding failure (Figure 35), revealing the importance of euphausiids in this species' diet, as well as the lack of euphausiids in our study area during 2005 and 2006. Since the breeding failures of 2005-06, euphausiids have increased in the auklet diet, and breeding success has also rebounded. In addition, the size class of euphausiids consumed matters. In warm water years, adult euphausiids that are consumed by auklets

are smaller and have less lipid content compared to the larger euphausiids available during cold water years.

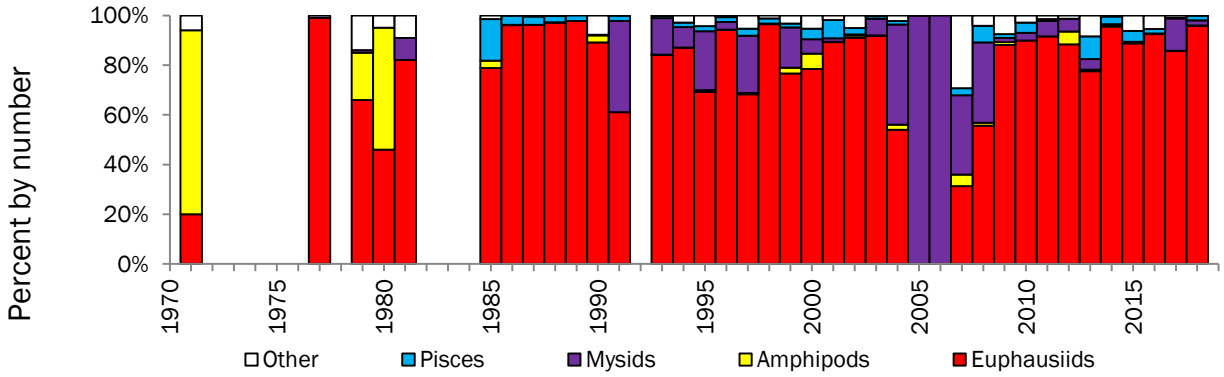

Figure 36. Cassin's auklet diet composition (through regurgitation analysis) on SEFI, 1971-2018.

Common murre

Brief species account

The common murre is a frequently-observed seabird in our study area and breeds on the Farallon Islands. They are an omnivorous seabird feeding mainly on fish, but they also consume zooplankton.

Abundance

In 2019, the peak density of common murres was recorded in May (35 murres/km^2; Figure 37). Since 2004, the highest abundance of murres was observed in May 2004 (64 murres/km^2). This species was abundant in 2004 and 2005, then declined in abundance in 2006. Densities of murres gradually increased over the next several years, then dropped in 2015. Recent counts could be indicative of another population growth period. In general, this species was present in higher number in spring and summer (i.e., May-July, the breeding months) than in the fall months.

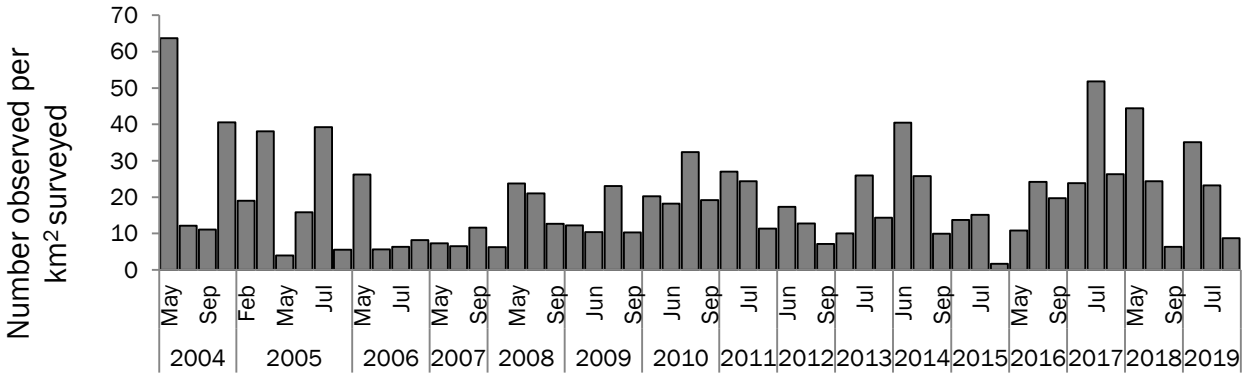

Figure 37. Abundances of common murres observed during each cruise, 2004-19.

Distribution

In 2019, common murres were distributed across the shelf of our study area, as well as some nearshore areas (Figure 38). In most years (e.g., 2004-06, 2008, 2010-13, not shown; Figure 38), murres were concentrated in areas between SEFI and Cordell Bank. In some years, this species was more dispersed, with more observations in the northern parts of the study area (e.g., 2005, 2009, 2014, and 2016 not shown) or further nearshore to the southeast area of SEFI (e.g., 2007-08, and 2014 not shown). Note that distributions shown here for years 2016-19 represent adult murre distributions; the 2018 results are from July (instead of May) and may represent common murre chicks, which typically do not start appearing in the waters of the sanctuaries until July and after.

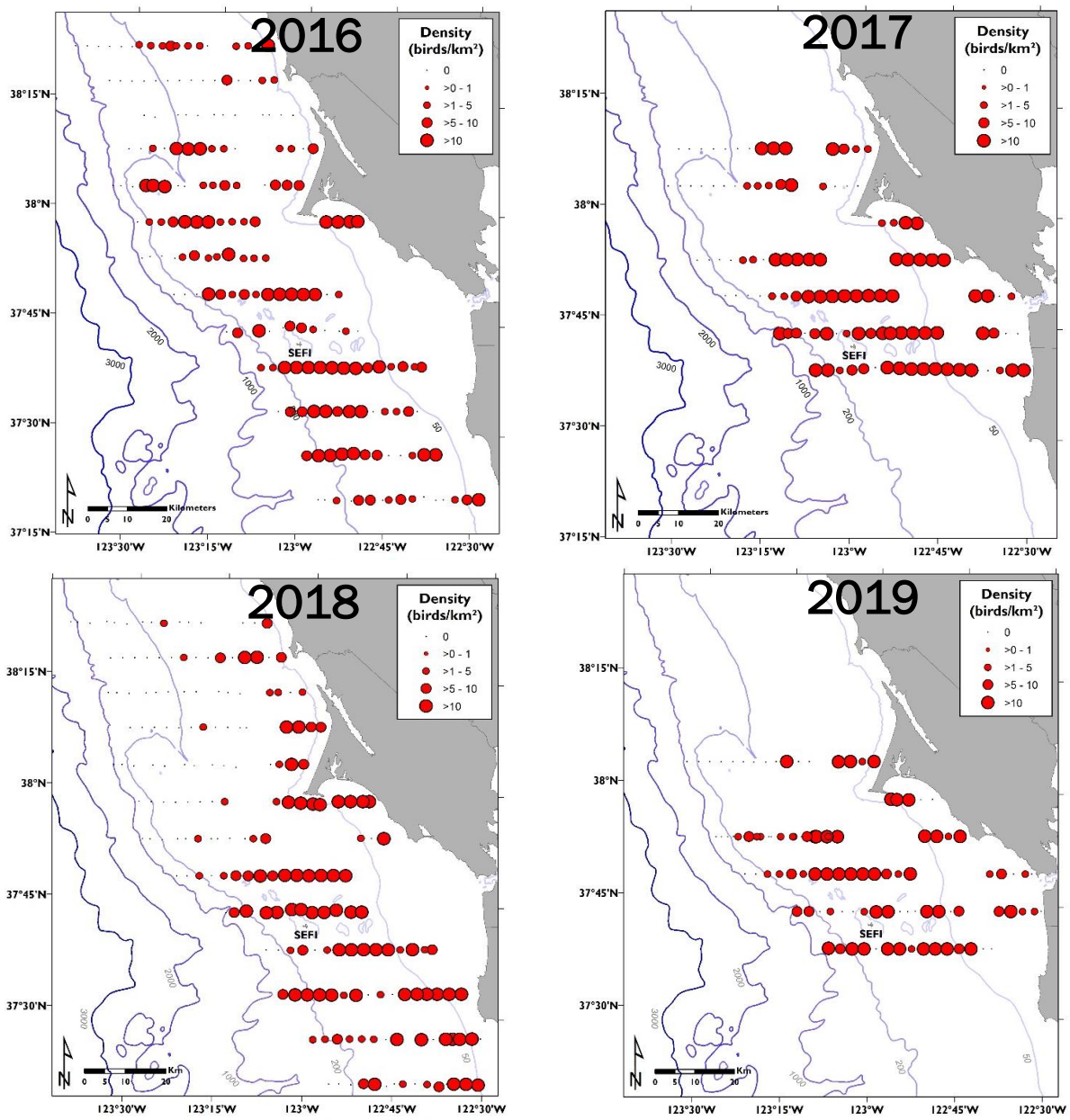

Figure 38. Common murre distributions during May or June, 2016-19.
NOTE: July 2018 is shown here, as the May survey only covered a small area.

Timing of breeding

Median egg laying date in 2019 was about 5 days later than the long-term average (Figure 39). Similar to the Cassin's auklet, we observed that common murres have later lay dates in poor ocean condition years (e.g., 1983, 1992, 1998, and 2015). Since 2004, the annual median lay date has hovered close to the long-term mean, with some years showing earlier lay dates (e.g., 2004, 2007, 2008, 2013) and some years showing later dates (e.g., 2005, 2006, 2010-11, 2015). There has been a slight trend in earlier lay dates through time, although this is not significant.

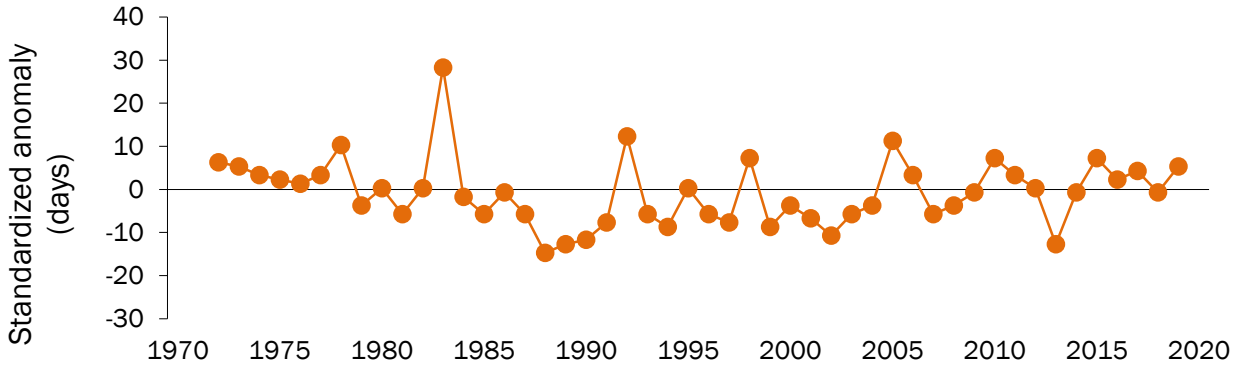

Figure 39. Common murre annual median egg lay dates on SEFI, 1972-2019.

Breeding success

Common murres experienced below-average breeding success (defined as chicks fledged per breeding pair) in 2019, a steep decline from the previous year (Figure 40). Similar to the Cassin's auklet, anomalously low productivity years (e.g., 1983, 1992, 1998) that punctuate the time series correspond to El Niño years, as well as years with late median lay dates (Figure 39). However, recent years of extremely low breeding success (i.e., 2006 and 2009) had relatively late median lay dates but were not El Niño years. Earlier lay dates (e.g., 1988; Figure 39) were linked to better productivity in some years, but this was not consistent; annual median lay dates for 2006 and 2009 were earlier compared to 2005, yet breeding success was worse. Some of these discrepancies in lay dates and productivity can be explained by low feeding rates to chicks, as observed in 2009.

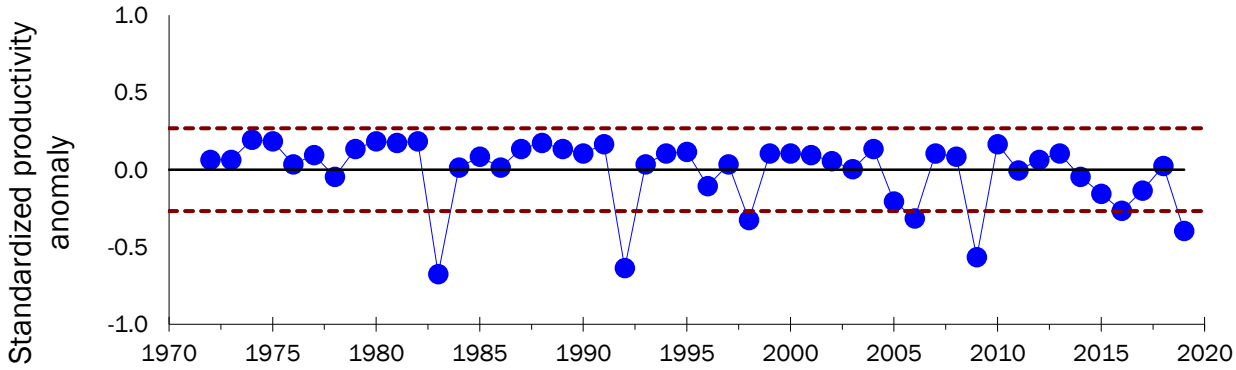

Figure 40. Common murre breeding success anomalies on SEFI, 1972-2019. Solid black line represents 48-year mean, and dotted red lines represent ±80% confidence intervals.

Diet

In 2019, common murre chicks on SEFI were fed mostly anchovy and sardine (Figure 41). Prey items being brought to common murre chicks have varied over time, with juvenile rockfish being the main diet items in the 1970s and 1980s, 2001-03, and 2009-17. Anchovy and sardine were the dominant prey in the 1990s, 2004-08, and again in 2018-19 (Figure 41). Historically, El Niño years corresponded to years with a low percentage of juvenile rockfish in the diet; these were also years of late timing of breeding (Figure 39) and low breeding success (Figure 40). However, 2005 and 2006 were not El Niño years, yet these years of poor ocean conditions (i.e. warm sea surface temperatures, weak alongshore

winds) yielded late breeding, low breeding success, and few rockfish in the murre diet. The 2009 results were exceptional, as murres were eating a lot of rockfish, yet breeding success was one of the lowest years on record; as mentioned previously, low chick feeding rates can help explain the low productivity in this year.

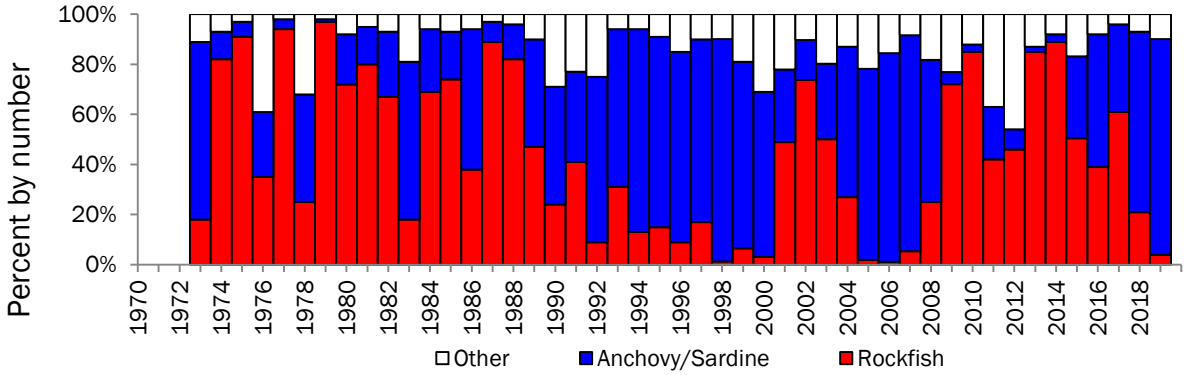

Figure 41. Common murre chick diet composition on SEFI, 1973-2019.

Brandt's cormorant

Brief species account

Brandt's cormorants are piscivorous birds found throughout the coastal areas of California. They are one of the breeding seabirds monitored on SEFI. In recent decades, Brandt's cormorants have been found to move from SEFI to mainland colonies (Ainley *et al.* 2018).

Abundance

Since 2007, Brandt's cormorants were observed in very low densities, and this trend has continued in 2019 (Figure 42). Numbers of Brandt's cormorants have declined through the time series, with the peak in October 2004 (12 cormorants/km^2); since this cruise, abundances have been less than half of this peak abundance. The October 2004 peak was later in the year compared to the high densities of other years, which generally occurred during the summer months (i.e., the breeding season). The low abundances observed in 2008-12 correspond to poor productivity for this species in these years, as well as a shift to mainland colonies (Ainley *et al.* 2018).

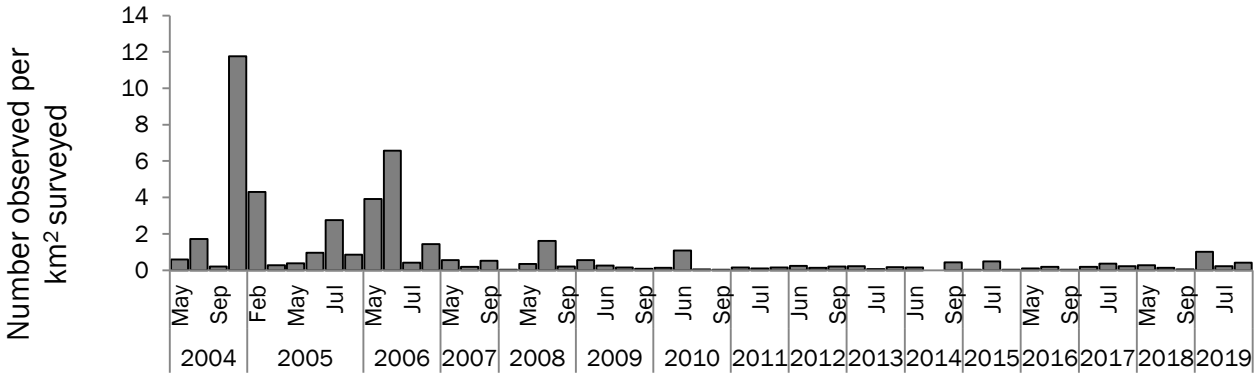

Figure 42. Abundances of Brandt's cormorants observed during each cruise, 2004-19.

Distribution

In 2019, Brandt's cormorants were observed east of SEFI and in nearshore waters (Figure 43). Brandt's cormorants have been observed near SEFI in most other years. In some years, this species was more scattered and observed in smaller groups or as individual birds in waters closer to shore (e.g., 2007, 2010, 2012-14 not shown; 2015 and 2017).

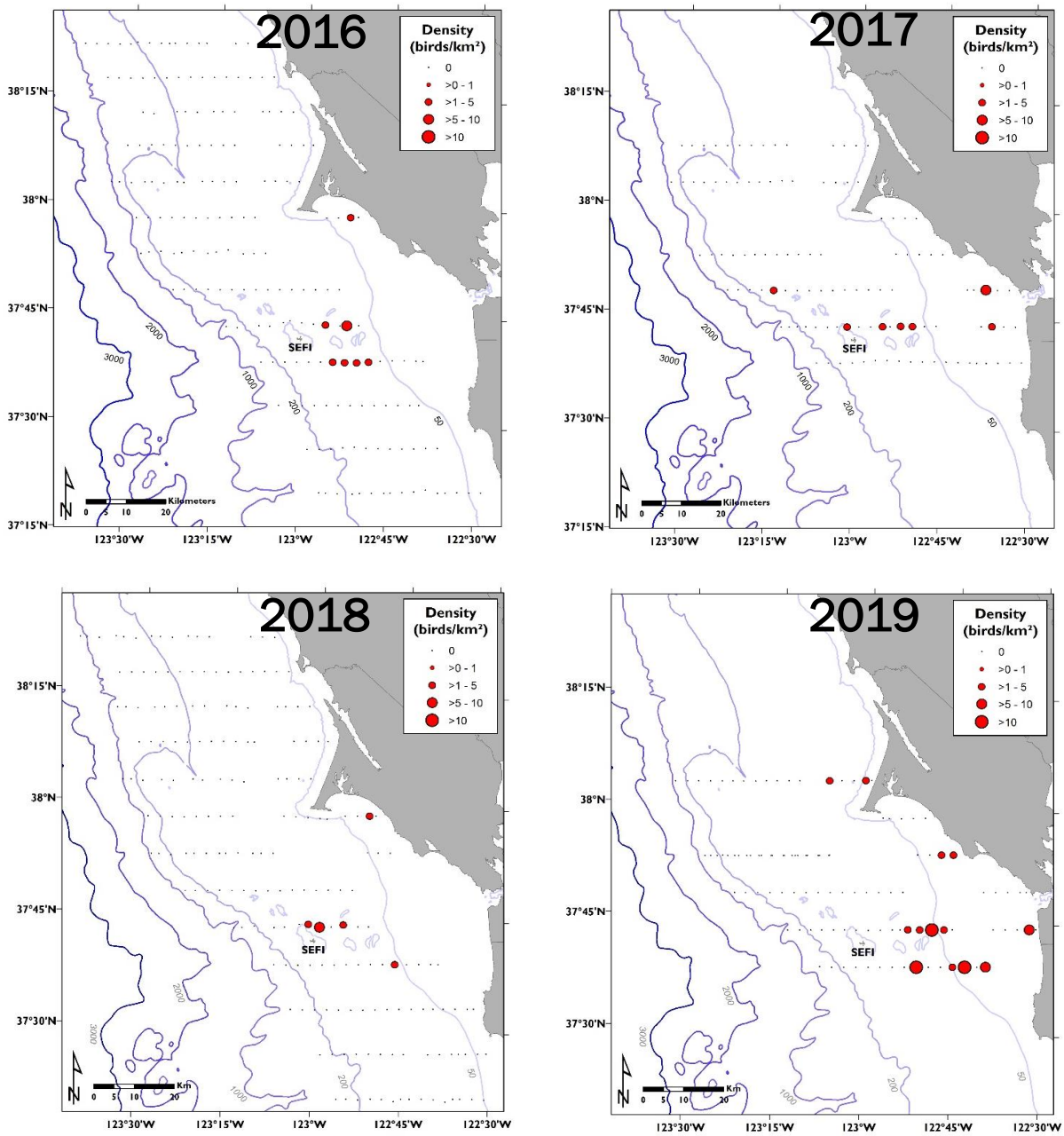

Figure 43. Brandt's cormorant distributions during May or June, 2016-19.
NOTE: July 2018 is shown here, as the May survey only covered a small area.

Timing of breeding

The median egg lay date for Brandt's cormorants on SEFI in 2019 was eight days later than the 48-year average (Figure 42). Timing of breeding in Brandt's cormorants isn't as clearly linked to ocean conditions as in Cassin's auklets or common murres; El Niño years (e.g., 1983, 1992, and 1998, 2015) do not show anomalously late lay dates. There has been a trend in later lay dates through time. Since 2004, this species began breeding early for three years (2004, 2006-07), and then bred late in 2005 and extremely late in 2008-12. The return to average median egg laying dates in the past six years has corresponded to improved breeding success (see below).

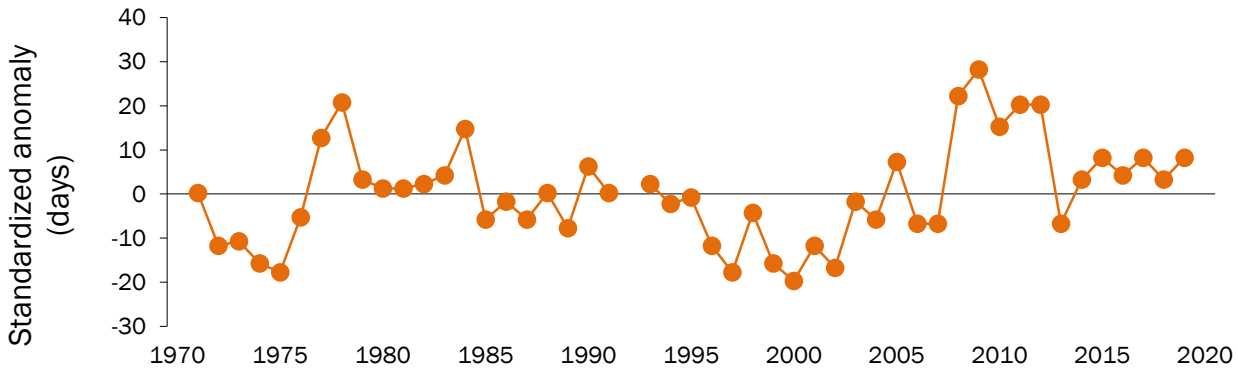

Figure 44. Brandt's cormorant annual median egg lay dates on SEFI, 1972-2019.

Breeding success

Breeding success of Brandt's cormorants on SEFI in 2019 was slightly above the long-term average (Figure 45). Most of the annual productivity estimates for Brandt's cormorants fall within the 80% forecast intervals around the long-term mean, similar to auklets and murres; however, unlike auklets and murres, Brandt's cormorants have experienced several years of extremely low productivity, usually corresponding to El Niño years (e.g., 1983, 1992). In looking at breeding success data since 2004, above average breeding success was observed in the first four years (2004-07), then extremely low productivity in 2007-12, very high in 2013-14, and now closer to average in the last five years.

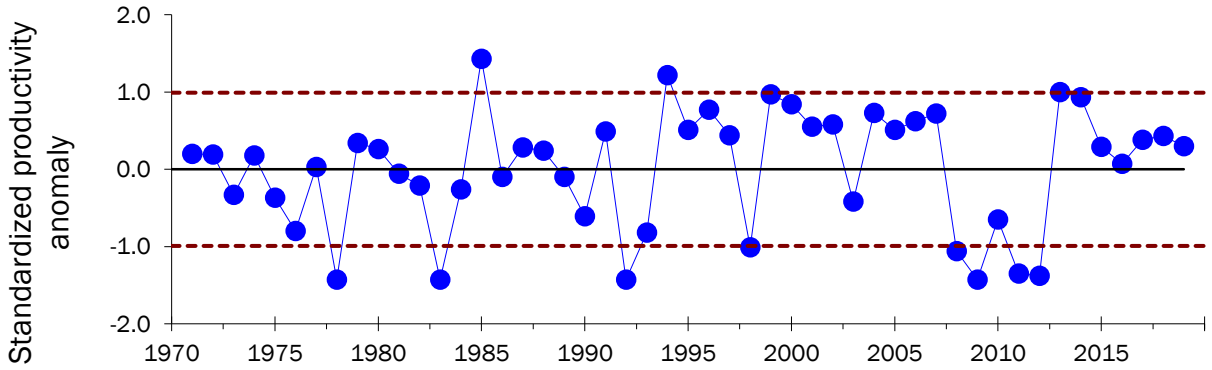

Figure 45. Brandt's cormorant breeding success anomalies on SEFI, 1971-2019. Solid black line represents 49-year mean, and dotted red lines represent ±80% confidence intervals.

Diet

The diet of Brandt's cormorants on SEFI has consisted of forage fishes (i.e., northern anchovy, Pacific sardine), various benthic species (i.e., sculpins, gobies, rockfish, and flatfish), and cephalopods. Brandt's cormorants on SEFI in 2019 consumed mostly northern anchovy (which has increased in the diet since 2015), while fewer rockfish and flatfish comprised their diet (Figure 46). Years with high percentages of anchovy and sardine in the diet (e.g., 1994, 2005-07) corresponded to years of high productivity, although higher breeding success has also correlated with high percentages of rockfish (e.g. 2013-14; Figure 46). Recent breeding success increases may be attributed to the increased

abundance of more offshore-distributed rockfish species which were likely absent during the poor productivity years (Elliott *et al.* 2015).

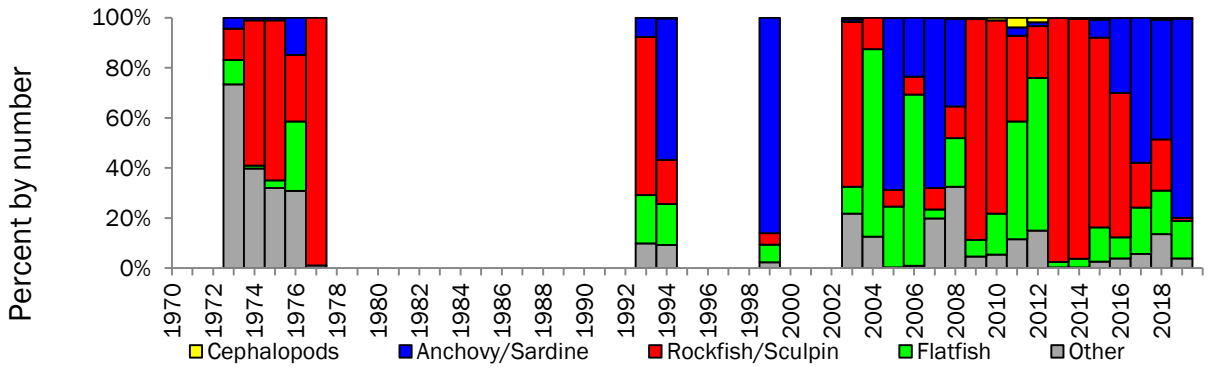

Figure 46. Brandt's cormorant diet composition on SEFI, 1994-2019. NOTE: Data for years 1973-77 from Ainley et al. 1981. Years 1999, 2004 and 2006 have low sample sizes.

Mammals

Overview

Marine mammals are top marine predators that feed on a variety of marine organisms. Some species breed within our study area, while other species migrate great distances to spend their non-breeding period in the central California Current. The abundances and distributions of marine mammals have been linked to bathymetric and hydrographic features that aggregate prey; many marine mammals live in or travel to the central California Current because of the highly-productive waters common to our study area. See the mammal observations section in the Appendix for details on these data.

Relative composition

There were 20 species of marine mammals observed during at-sea cruises since 2004 (Table 3). The fifteen most abundant marine mammal species include two known SEFI residents: California sea lion and Steller sea lion; both of these species are piscivorous. Risso's dolphin, Pacific white-sided dolphin, Dall's porpoise, and northern right whale dolphin all consume fish and squid, and are known to inhabit offshore waters. The two most abundant whale species (humpback and blue) are both euphausiid-consuming whales that are common to coastal and shelf waters.

Table 3. Marine mammal species and average densities per cruise, 2004-19.

Common name	Average density (#/km of surveyed distance)	Common name	Average density (#/km of surveyed distance)
California sea lion	0.2306	killer whale	0.0029
Humpback whale	0.2009	northern elephant seal	0.0024
Pacific white-sided dolphin	0.1345	harbor seal	0.0017
Risso's dolphin	0.1298	fin whale	0.0009
Dall's porpoise	0.0799	Guadalupe fur seal	0.0008
unidentified whale	0.0748	unidentified cetacean	0.0007
northern right whale dolphin	0.0559	unidentified porpoise	0.0006
unidentified otariid	0.0264	gray whale	0.0005
blue whale	0.0256	common minke whale	0.0005
unidentified dolphin	0.0187	unidentified fur seal	0.0004
short-beaked common dolphin	0.0137	unidentified sea lion	0.0003
unidentified pinniped	0.0112	common dolphin (undifferentiated)	0.0002
northern fur seal	0.0093	sperm whale	0.0001
Steller sea lion	0.0089	bottlenose dolphin	0.0001
harbor porpoise	0.0075		

In the following sections, more detailed information will be provided on the two common migrant whales observed in our study area: humpback whale and blue whale.

Humpback whale

Brief species account

Humpback whales are found in groups along the coast of western North America. The humpback whales visiting the California coast belong to three distinct population segments designated by NOAA: those that overwinter in Mexico (threatened), Central America (endangered), and Hawaii-Alaska (Calambokidis *et al*. 2001). These whales spend the summer months along the coast from Alaska to California, moving south (e.g., Mexico and Central America) during the winter. This species feeds mainly on euphausiids but will also consume fish.

Abundance

Humpback whale abundance peaked in September (0.64 whales/km) in 2019, which was the fourth highest density in the time series (Figure 47). While peak numbers of this species are typically seen in the fall (Sep-Oct), the warm-water conditions in the study area in 2014-15 may have led to an earlier peak for these whales (as well as in 2010-11). The poor ocean conditions in 2005-06 could explain why there were relatively fewer whales. The improved conditions in 2007-12 and 2016-19 have led to higher densities of this species, while lower abundances were observed in 2013-15.

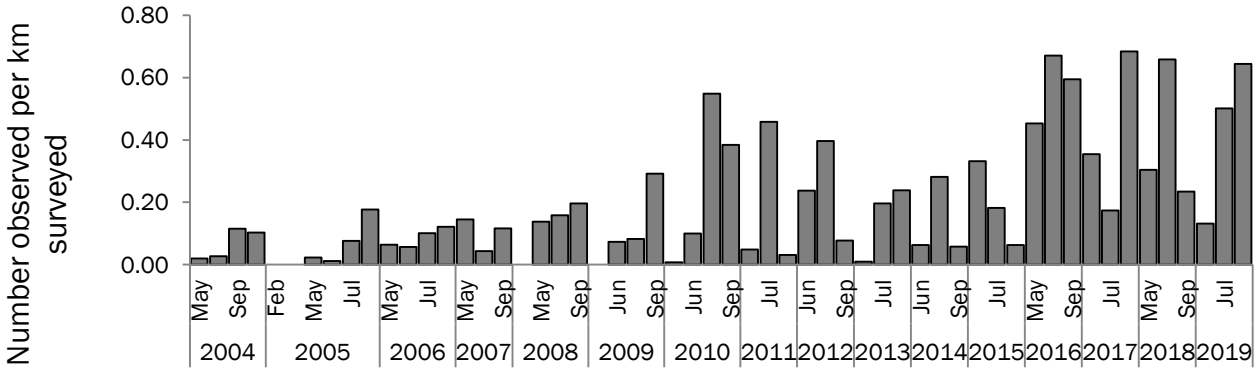

Figure 47. Humpback whale abundances, 2004-19.

Distribution

Humpback whales were sighted over the shelf in 2019, with some nearshore sightings in May and July (Figure 48). In 2004-06 and 2014 (not shown), this species congregated on the shelf and near SEFI in earlier months (May-July), and then expanded north to Cordell Bank and near the 200 m isobath in the fall (Sept-Oct). In 2007-09 (not shown), the distributions changed; humpback whales were consistently observed on the shelf throughout the study area, with some aggregations in inshore areas and near SEFI. In 2010-13 (not shown), small numbers of this species were observed in early months (mainly near the shelf break), while greater numbers of whales were observed over Cordell Bank and on the shelf in later months; 2012 (not shown) was an exception, with higher numbers observed in June in nearshore areas.

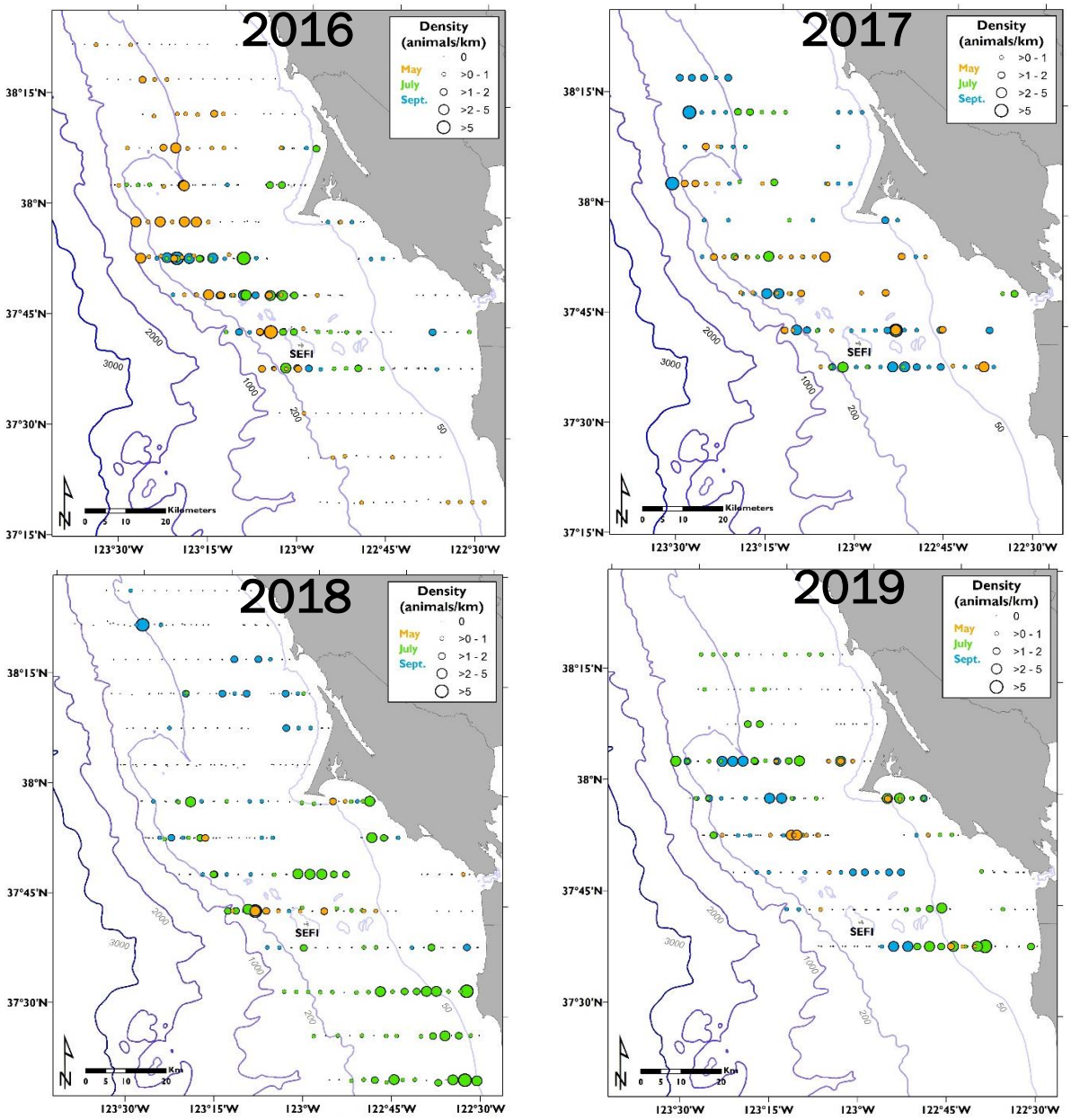

Figure 48. Humpback whale annual distributions, 2016-19.

Blue whale

Brief species account

The blue whale is the largest animal on earth, and it feeds on euphausiids (and occasionally other invertebrates). This species is found in all the oceans, and calves are found in tropical and subtropical waters during winter months. This species is found off the coast of California during the summer.

Abundance

The peak abundance of blue whales in 2019 was observed in September (0.07 whales/km), while no blue whales were observed in July 2019 (Figure 49). The highest density (0.16 whales/km) was observed in July 2016. In most years, blue whales have peaked in abundance in late summer and early fall months (July-Oct). The delayed upwelling in 2005 may have led to a delay in peak densities, and the lack of blue whales in 2006 was evidence of the poor ocean conditions. Despite the improved conditions in 2007-09, observations of this species remained relatively low and remained at low abundances through 2014; increased densities were observed again in 2015-18.

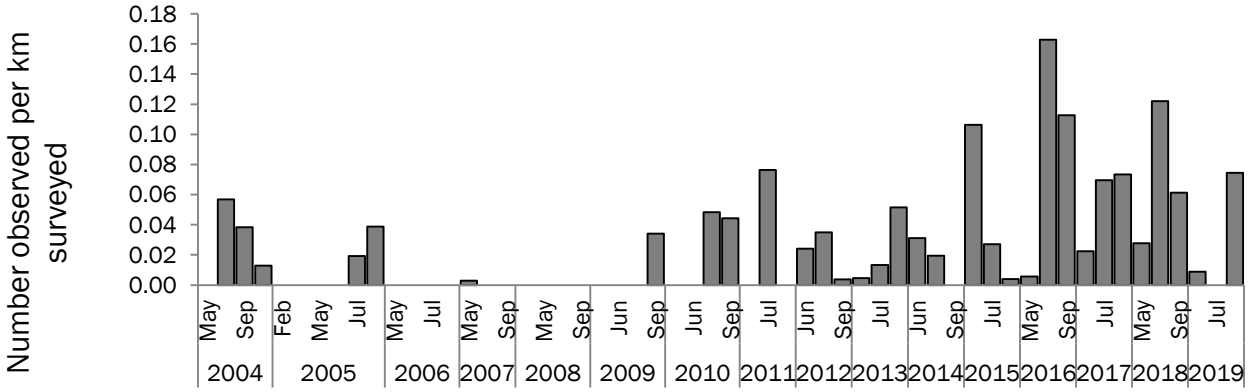

Figure 49. Blue whale abundances, 2004-19.

Distribution

In 2019, blue whales were observed in small numbers near Cordell Bank in May and Sept (Figure 50). The September findings are more consistent with colder water years (e.g. 2007, 2009-11, not shown), while May and July results were similar to warm water years (e.g. 2014-15, not shown). Blue whales have been found in the northern part of the study area (over Cordell Bank) in 2004-05 and 2013 (not shown). Blue whale sightings were scattered on the shelf in 2012 (not shown) and 2017-18 (Figure 50).

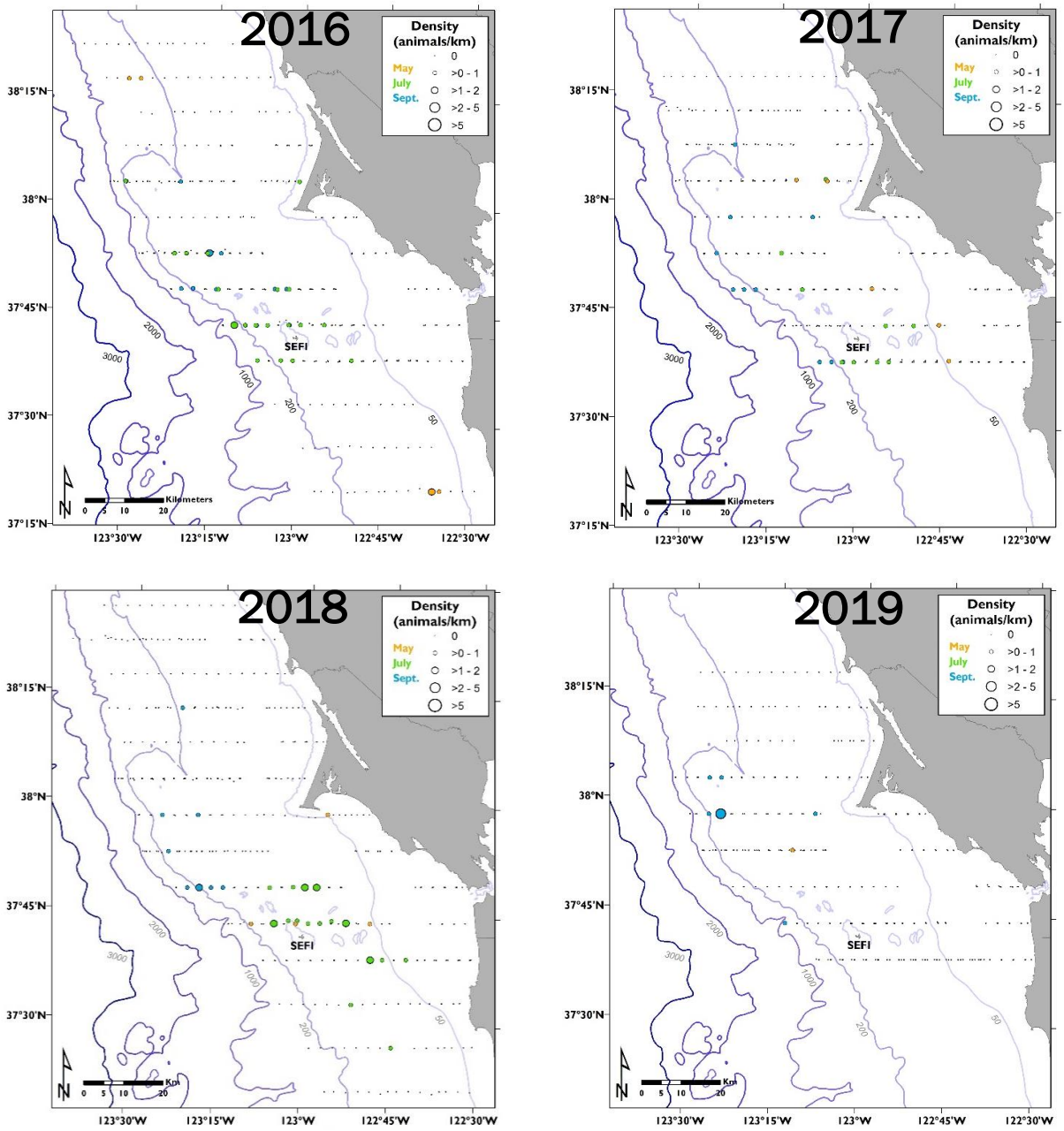

Figure 50. Blue whale annual distributions, 2016-19.

Blue whales and euphausiid abundance

Annual estimates of blue whale abundance in the core area of our transect grid (lines 1-7) generally follow patterns in the abundance of euphausiids. Euphausiids are the main prey of blue whales, and euphausiid biomass is estimated using acoustics (Figure 51). Some years show agreement of predator and prey abundances (e.g. 2007, 2010), while other years show discrepancies with euphausiids in deeper waters (e.g. 2006, 2016) and euphausiids in shallower waters (e.g. 2013, 2015, 2017). Euphausiid estimates for 2006 are likely unreliable due to the high abundance of jellies, which produce a similar acoustic signal to masses of euphausiids.

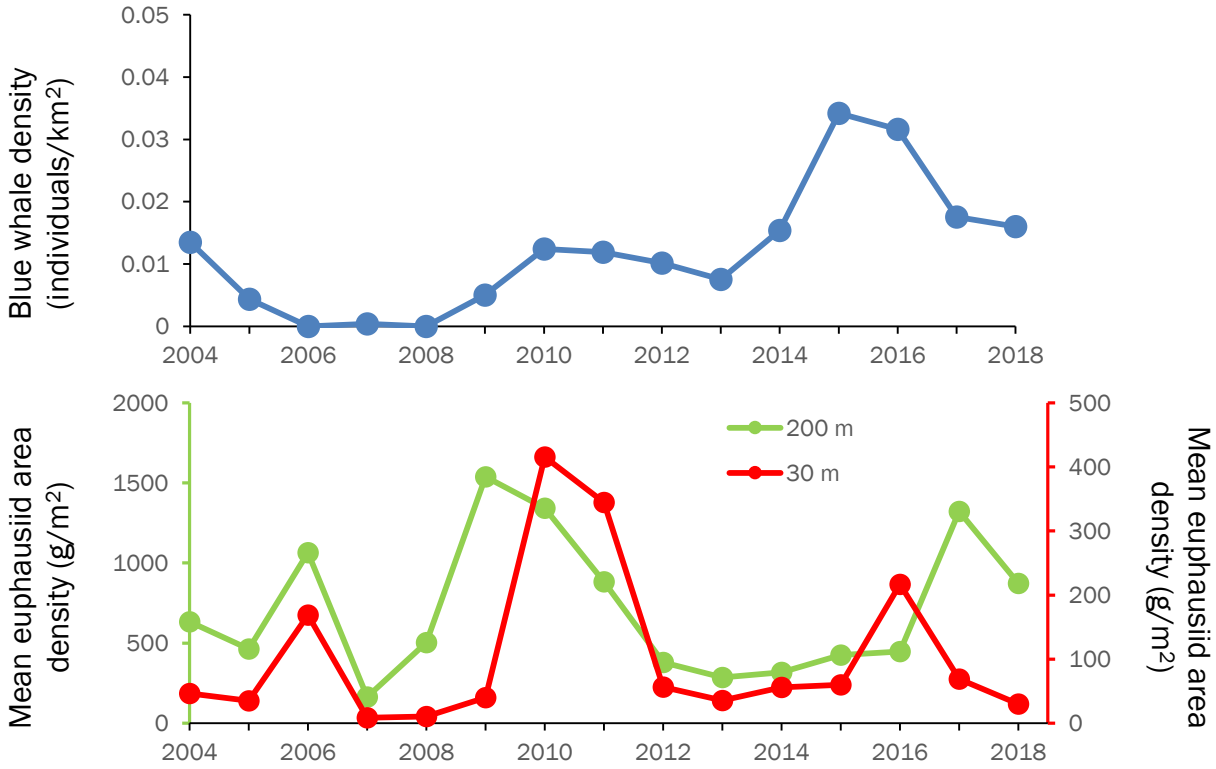

Figure 51. Blue whale (top) and euphausiid (bottom) densities in the core ACCESS study area (lines 1-7), 2004-18.

Humpback whales and euphausiid abundance

Annual estimates of humpback whale abundance in the core area of our transect grid (lines 1-7) generally follow similar patterns in the abundance of their euphausiid prey (estimated using acoustics; Figure 52). Some years show agreement of predator and prey abundances (e.g. 2010, 2016), while other years show discrepancies with euphausiids in both deep and shallow waters (e.g. 2006, 2012). Euphausiid estimates for 2006 are likely unreliable due to the high abundance of jellies, which produce a similar acoustic signal to masses of euphausiids.

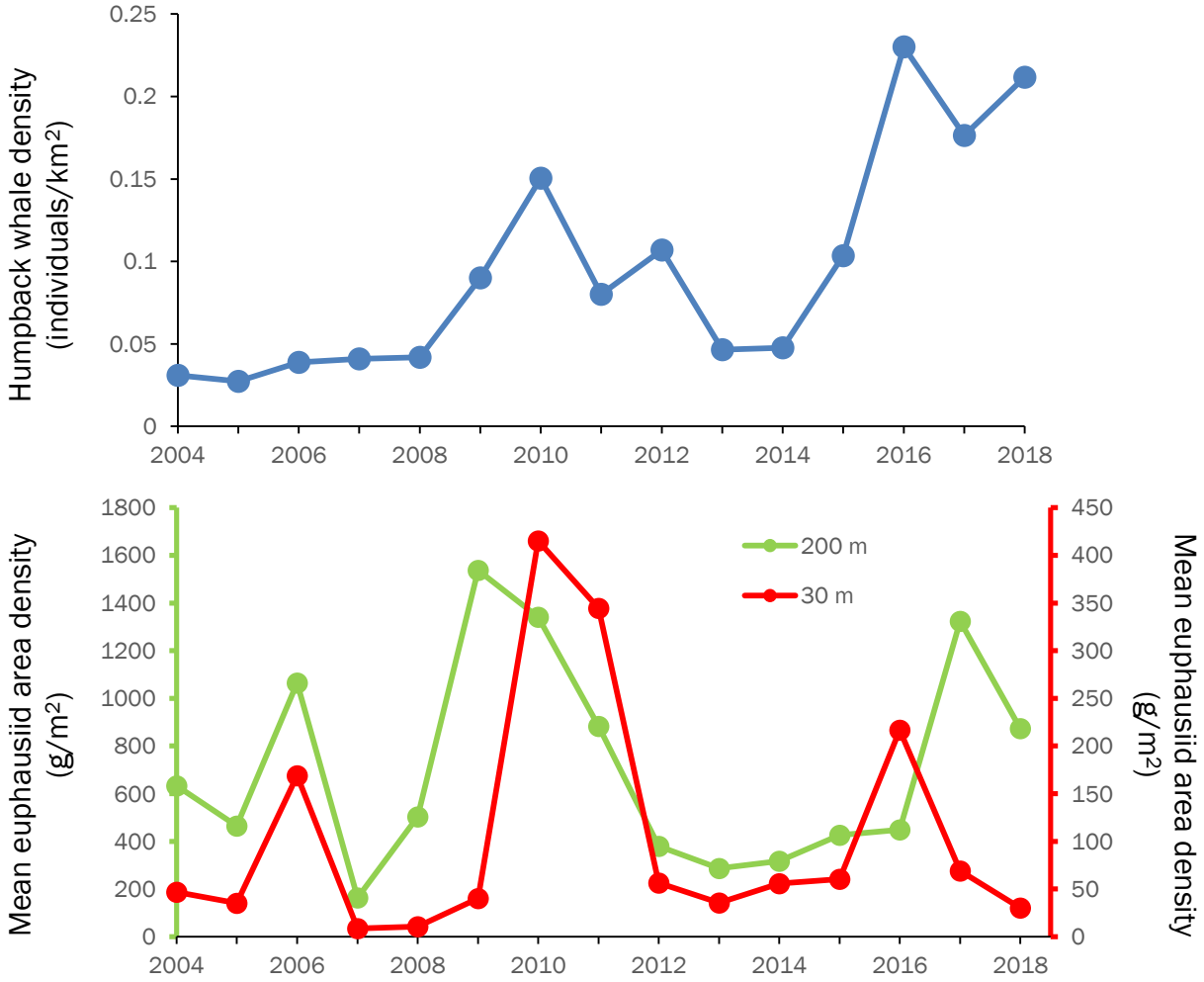

Figure 52. Humpback whale (top) and euphausiid (bottom) densities in the core ACCESS study area (lines 1-7), 2004-18.

CONCLUSIONS

In 2019, the ACCESS partnership completed its 16th year of monitoring, with a total of 58 cruises to date. The spring transition to the upwelling season in 2019 was late; relaxed, warm water conditions prevailed for the year, with intermittent upwelling periods during the fall. Euphausiids were larger compared to 2018. Breeding success of seabirds on the Farallones was anomalously poor for the Cassin's auklet and common murre; Brandt's cormorants were slightly above the long-term average. Compared to 2018, seabirds and whales were generally seen in smaller numbers. Compared to the long-term averages, seabirds were below average in 2019 while whales were above the long-term average.

Physical ocean climate indicators illustrated poor ocean conditions for most of 2019, with improving conditions in the latter part of the year (Table 1). Climate indices, such as the Southern Oscillation Index (SOI) and the North Pacific Gyre Oscillation (NPGO), indicated warm, low productivity conditions for the year. Alongshore winds were weak in the early months, followed by average to strong winds. Upwelling indices were mixed depending on the source, showing weak upwelling (on a local scale) and either strong upwelling or pulses of upwelling and relaxation throughout the year (on a regional scale). Sea surface heights were elevated throughout the year, suggesting downwelling conditions. Spring transition date was late. Sea surface temperature showed an overall warm regime for the year, with a local buoy showing cooler conditions in the fall months. Sea surface salinity values were above average in the early months, followed by average values; nutrient concentrations were low except in May.

Biological ocean climate indicators echo results from the physical indicators in some cases, but not in others (Table 1). Starting at the base of the marine food web, phytoplankton abundance (as indicated by chlorophyll a concentrations) showed low to average abundances for the first half of the year. Phytoplankton community results indicated a diatom-dominated community in early 2019, followed by a dinoflagellate-dominated community. Zooplankton community composition results are not yet available for 2016-19. We show results from 2004-15. The most recent results from 2015 reflect overall high abundances of zooplankton compared to warm, poor productivity years (e.g. 2004-06), particularly for copepods and the "other" category (which is mostly comprised of gelatinous species). We examined copepods, pteropods, and euphausiids in more detail, as these are important low- to mid-trophic level species in the ecosystem. Euphausiid biomass (as measured by acoustics) is not yet available for 2019; warm water conditions, which generally show a decline in the percentage of adult stages, although 2019 (a warm year) was an exception and showed relatively high abundances of adult euphausiids. Additionally, adult euphausiids are larger in cold water years (e.g. 2007-13) and smaller in warm water years (e.g. 2005-06, 2014-16); adults in 2019 were larger than adults in 2018, indicative of the transition out of the North Pacific marine heat wave.

The top-level predators in our region are represented by three resident breeding seabirds and two migrant whales. Cassin's auklet, a zooplanktivorous seabird, was observed foraging primarily over Cordell Bank in 2019; the average egg laying date was slightly later for this species and experienced anomalously low breeding success. An omnivorous seabird species, the common murre, foraged across the shelf in 2019, had a slightly later egg laying

date, experienced very low breeding success, and consumed mostly anchovy and sardine. Brandt's cormorants are piscivorous and were observed in low numbers near SEFI and nearshore waters in 2019. This species had a slightly later start to breeding, experienced somewhat above-average productivity, and consumed mostly anchovy in 2019. For our marine mammal climate indicator species in 2019, humpback whales were observed in high numbers; they were spotted over the continental shelf. Blue whales were observed in relatively low numbers in 2019 compared to the previous year; they appeared near Cordell Bank in May and September. Both species showed peak numbers in September 2019.

Table 1. Summary of 2019 conditions as determined by physical and biological indicators.

Indicator Name (*scale*)	2019 Conditions
Physical Indicators	
Southern Oscillation Index	Poor
Pacific Decadal Oscillation	Average
North Pacific Decadal Oscillation	Poor
Wind	Poor
Sea surface height	Poor
Upwelling (BB) – *local*	Poor
Upwelling (PFEL) – *regional*	Good
Upwelling (CUTI) – *regional*	Average
Spring transition (BB) – *local*	Good
Spring transition (PFEL) – *regional*	Good
Sea surface temperature (BB) – *local*	Average
Sea surface temperature (SEFI) – *local*	Poor
Sea surface temperature (Satellite) – *regional*	Poor
Sea surface salinity	Average
Aragonite saturation	Poor
Dissolved oxygen	Average
Nitrates (NO_3) and Nitrites (NO_2)	Poor
Phosphates (PO_4)	Poor
Silicates (Si)	Poor
Biological Indicators	
Chlorophyll a	Good
Phytoplankton composition	Poor
Zooplankton composition	Data not available
Copepods	Data not available
Pteropods	Data not available
Euphausiids – Acoustics	Data not available
Euphausiids – Age classes	Good
Euphausiids – Adult sizes	Average
Cassin's auklet – at-sea numbers	Poor
Cassin's auklet – egg laying date	Average
Cassin's auklet – breeding success	Poor
Cassin's auklet – diet	Data not available
Common murre – at-sea numbers	Average
Common murre – egg laying date	Average

Common murre – breeding success	Poor
Common murre – diet	Poor
Brandt's cormorant – at-sea numbers	Poor
Brandt's cormorant – egg laying date	Average
Brandt's cormorant – breeding success	Good
Brandt's cormorant - diet	Good
Humpback whale – at-sea numbers	Good
Blue whale – at-sea numbers	Average

Marine heatwaves

The last marine heatwave that impacted our study area was the North Pacific marine heatwave of 2014-16. Local and regional physical attributes showed increased sea surface temperatures, weak alongshore winds, increased sea level height, weak upwelling conditions, and low concentrations of key nutrients in surface waters. Our local zooplankton community (as shown through hoop net samples) shifted towards a gelatinous-dominated community different from past warm water regimes, with increased abundances of tunicates and doliolids, and a near absence of pteropods. Acoustics data showed reduced local krill abundance, while adult krill shrunk in size and young age classes of krill dominated Tucker trawl samples.

Higher trophic levels were impacted by these changes as well. Cassin's auklets experienced above average breeding success during the heatwave; however, a tagging study showed this species traveling farther during the winter to find their prey (Johns *et al*. 2020). Humpback whales arrived to our study area earlier than most other years, and due to the lack of krill (their main prey item), this species spent more time in nearshore areas and became entangled in crab pot gear much more frequently than in past years.

From physical to biological indicators, the marine heatwave of 2014-16 had many impacts to the marine ecosystem. These findings highlight the importance of the ACCESS program in monitoring these oceanographic regimes. As future heatwaves develop, ACCESS is well-suited to track these changes, share data with other scientists, and help managers navigate the changing marine environment. For example, we now know that humpback whales will likely move to nearshore waters to feed during marine heatwaves and increase their likelihood of being entangled in crab pot fishing gear; when we observe the beginning of a heatwave, managers can work more closely with the California Department of Fish and Wildlife and crab fishermen to adjust fishing practices to save whales from entanglements.

Importance of the ACCESS program

ACCESS's long term monitoring of oceanographic conditions, prey availability, and the distribution and abundance of top marine predators is valuable for understanding local and regional conditions, as well as the effects of climate change that will be bringing changes in temperature, sea level rise, and ocean chemistry (to name a few). ACCESS data help us gauge the severity of large scale phenomena (e.g. The Blob, El Niño) on our local marine

resources. With this information, we can manage additional human stressors to mitigate the effects of climate change.

The ACCESS data are also being used to provide timely, relevant ecosystem data for management issues in our national marine sanctuaries and addresses many of the sanctuaries management priorities. ACCESS data helps reduce threats to key species by identifying wildlife hotspots and trends. ACCESS informs management of risks to whales from ship strikes and entanglement and develops actions to reduce risk. ACCESS data helps assess resources at risk from changing climate by helping management to understand how our sanctuary ecosystem is changing, by monitoring oceanographic conditions. ACCESS expands the recognition and outreach of national marine sanctuaries through traditional media, social media, events, presentations, publications and involving students, interns and Teachers At Sea, providing hands-on research. ACCESS was created through strong alliances and partnerships between state and federal marine resource agencies, academic and non-government research institutions. At its core, ACCESS tracks and predicts conditions and trends of ecosystem services and synthesizes our findings for management and the public.

The data collected informs marine resource managers about impacts to wildlife and their food webs from a changing marine environment. Understanding impacts from climate change and large scale phenomena inform management decisions and help prepare resource managers for future ocean conditions. Marine resource managers use long-term data trends to assess the effectiveness of marine resource policy and identify needs for management actions. For example, Greater Farallones and Cordell Bank national marine sanctuaries use ACCESS data to guide policy on reducing ship strikes to endangered and threatened whales. Through models using the ACCESS data, researchers analyze the potential effectiveness of different strategies to reduce the co-occurrence of blue, fin, and humpback whales with large ships. Point Blue uses ACCESS data to identify important wildlife feeding areas which inform marine spatial management such as the location of potential wind farms and potential whale interaction with crab pots. The California Department of Fish and Wildlife uses the data to reduce whale entanglement. Non-profits use the data on the location of out-of-season crab pots to focus derelict crab pot removal activities. These are examples of how marine resource managers use ACCESS data for greater wildlife conservation, informed ocean zoning, and understanding impacts from increased CO_2 in the atmosphere. ACCESS was created through strong alliances and partnerships among state and federal marine resource agencies, academic and non-government research institutions. At its core, ACCESS tracks and predicts conditions and trends in the north-central California national marine sanctuaries and synthesizes the findings for management and the public to inform actions for a healthy and productive marine environment.

REFERENCES

Ainley DG, Anderson DW, Kelly PR. 1981. Feeding ecology of marine cormorants in southwestern North America. *Condor* 83: 120-131.

Ainley DG, Santora JA, Capitolo PJ, Field JC, Beck JN, Carle RD, Donnelly-Greenan E, McChesney GJ, Elliott M, Bradley RW, Lindquist K, Nelson P, Roletto J, Warzybok P, Hester M, Jahncke J. 2018. Ecosystem-based management affecting Brandt's Cormorant resources and populations in the central California Current region. *Biological Conservation* 217: 407-418.

Becker BH, Peery MZ, Beissinger SR. 2007. Ocean climate and prey availability affect the trophic level and reproductive success of the marbled murrelet, an endangered seabird. *Marine Ecology Progress Series* 329: 267-279.

Bran and Luebbe Inc. 1999a. Bran Luebbe AutoAnalyzer Applications: AutoAnalyzer Method No. G-172-96 nitrate and nitrite in water and seawater. Buffalo Grove, IL: Bran and Luebbe Inc.

Bran and Luebbe Inc. 1999b. Bran Luebbe AutoAnalyzer Applications: AutoAnalyzer Method No. G-175-96 phosphate in water and seawater. Buffalo Grove, IL: Bran and Luebbe Inc.

Bran and Luebbe Inc. 1999c. Silicate in water and seawater. AutoAnalyzer Method No. G-177-96. Buffalo Grove, IL: Bran and Luebbe Inc.

Calambokidis J, Steiger G, Straley JM, Herman LM, Cerchio S., Salden DR, Urban J, Jacobsen JK, von Ziefersar O, Balcom KC, Gabriele CM, Dahlheim M, Uchida S, Ellis G, Miyamura Y, Ladron de Guevara P, Yamaguchi M, Mizroch SA, Schlender L, Rasmussen K, Barlow J, Quinn TJ. 2001. Movements and population structure of humpback whales in the North Pacific. *Marine Mammal Science* 17(4): 769-794.

Dahdul WM, Horn MH. 2003. Energy allocation and postnatal growth in captive elegant tern (*Sterna elegans*) chicks: responses to high- versus low-energy diets. *The Auk* 120(4): 1069-1081.

Davis CV, Hewet K, Hill TM, Largier JL, Gaylord B, Jahncke J. 2018. Reconstructing aragonite saturation state based on an empirical relationship for northern California. Publication in preparation, Estuaries and Coasts. https://doi.org/10.1007/s12237-018-0372-0

Duncan BE, Higgason KD, Suchanek TH, Largier J, Stachowicz J, Allen S, Bograd S, Breen R, Gellerman H, Hill T, Jahncke J, Johnson R, Lonhart S, Morgan S, Roletto J, Wilkerson F. 2013. *Ocean Climate Indicators: A Monitoring Inventory and Plan for Tracking Climate Change in the North-central California Coast and Ocean Region.* Report of a Working Group of the Gulf of the Farallones National Marine Sanctuary Advisory Council. 74pp. http://farallones.noaa.gov/manage/climate/pdf/GFNMS-Indicators-Monitoring-Plan-FINAL.pdf

Elliott ML, Bradley RW, Robinette DP, Jahncke J. 2015. Changes in forage fish community indicated by the diet of the Brandt's cormorant (*Phalacrocorax penicillatus*) in the central California Current. *Journal of Marine Systems* 146: 50-58.

Fontana RE, Elliott ML, Largier JL, Jahncke J. 2016. Temporal variation in zooplankton abundance and composition in a strong, persistent coastal upwelling region. *Progress in Oceanography* 142: 1-16.

Frederickson M, Anker-Nilssen T, Beaugrand G, Wanless S. 2013. Climate, copepods and seabirds in the boreal Northeast Atlantic – current state and future outlook. *Global Change Biology* 19: 364-372.

Hutto SV, editor. Climate-Smart Adaptation for North-central California Coastal Habitats. Report of the Climate-Smart Adaptation Working Group of the Greater Farallones National Marine Sanctuary Advisory Council. San Francisco, CA. 47 pp. https://nmsfarallones.blob.core.windows.net/farallones-prod/media/archive/manage/climate/pdf/Climate-SmartAdaptationReport.pdf

Johns ME, Warzybok P, Jahncke J, Lingberg M, Breed GA. 2020. Oceanographic drivers of winter habitat use in Cassin's Auklets. *Ecological Applications* 30(3), e02068.

MacDonald RW, McLaughlin FA, Wong CS. 1986. The storage of reactive silicate samples by freezing. Limnology and Oceanography 31: 1139-1142.

Mackas D, Galbraith M. 2002. Zooplankton distribution and dynamics in a North Pacific eddy of coastal origin: I. Transport and loss of continental margin species. *Journal of Oceanography* 58, 725–738.

Mackas D. Tsurumi M, Galbraith M, Yelland D. 2005. Zooplankton distribution and dynamics in a North Pacific Eddy of coastal origin: II. Mechanisms of eddy colonization by and retention of offshore species. *Deep Sea Research Part II: Topical Studies in Oceanography* 52, 1011–1035.

Postel L, Fock H, Hagen W. 2000. Biomass and abundance. In: Harris R, Wiebe P, Lenz J, Skjoidal H, Huntley M (Eds.), ICES Zooplankton Methodology Manual, Academic Press, San Diego, CA. pp. 83-192.

Whitledge TE, Malloy SC, Patton CJ, Wirick CD. 1981. Automated nutrient analyses in seawater. Brookhaven Natl. Lab. Formal Rep. BNL 51398.

APPENDIX: DATA AND METHODS

Overview

The results shown in this report provide a comprehensive view of the physical and biological ocean climate indicators in our study region. Some indicators are generated through data collected during ACCESS cruises, while others are obtained from online sources to provide context. Many of the variables are shown in figures as anomalies. Anomalies are derived from the long-term dataset, and bar graphs show the deviation of each year, month, or seasonal variable from the long-term mean.

Online data

Below are descriptions of the data obtained online and various data processing steps.

Southern Oscillation Index (SOI)

- *Source*: http://www.cgd.ucar.edu/cas/catalog/climind/SOI.signal.txt
  - The Southern Oscillation Index characterizes the large scale sea level pressure patterns in the tropical Pacific. More information can be found here: https://climatedataguide.ucar.edu/climate-data/southern-oscillation-indices-signal-noise-and-tahitidarwin-slp-soi
- Data used in Figure 2.
- *Data processing*:
  - Monthly indices are downloaded.
  - Long-term (1866-present) monthly averages are calculated.
  - The long-term monthly averages are subtracted from the monthly indices to obtain the monthly anomalies.
  - 99% confidence intervals are calculated based on the long-term monthly means.

Pacific Decadal Oscillation (PDO)

- *Source*: http://research.jisao.washington.edu/pdo/PDO.latest.txt
  - The Pacific Decadal Oscillation (PDO) Index is defined as the leading principal component of North Pacific monthly sea temperature variability (poleward of 20N). More information can be found here: http://research.jisao.washington.edu/pdo/
- Data used in Figure 3.
- *Data processing*:
  - Monthly indices are downloaded.
  - Long-term (1900-present) monthly averages are calculated.
  - The long-term monthly averages are subtracted from the monthly indices to obtain the monthly anomalies.
  - 99% confidence intervals are calculated based on the long-term monthly means.

North Pacific Gyre Oscillation (NPGO)

- *Source*: http://www.o3d.org/npgo/npgo.php

    - The North Pacific Gyre Oscillation (NPGO) is a climate pattern that emerges as the second dominant mode of sea surface height variability in the Northeast Pacific and is significantly correlated with previously unexplained fluctuations of salinity, nutrients, and chlorophyll a. More information can be found here: http://www.o3d.org/npgo/
- Data used to make Figure 4.
- *Data processing*:
    - Monthly indices are downloaded.
    - Long-term (1950-present) monthly averages are calculated.
    - The long-term monthly averages are subtracted from the monthly indices to obtain the monthly anomalies.
    - 99% confidence intervals are calculated based on the long-term monthly means.

NOAA Bodega Bay buoy data (Station 46013)

- *Sources*:
    - Bodega Bay buoy (38.253 N 123.303 W): https://www.ndbc.noaa.gov/station_history.php?station=46013
    - San Francisco buoy (37.754 N 122.839 W): https://www.ndbc.noaa.gov/station_history.php?station=46026
    - Half Moon Bay buoy (37.356 N 122.881 W): https://www.ndbc.noaa.gov/station_history.php?station=46012
    - We use the meteorological data; data descriptions and units can be found here: https://www.ndbc.noaa.gov/measdes.shtml
- Data used in Figures 5, 7, 11, and 12.
- *Data processing:*
    - Each year of buoy data is downloaded as a .txt file, opened in Excel, and a macro is run that does the following:
        - Decomposes the wind vector into zonal (i.e., east-west coordinate) and meridional (i.e., north-south coordinate) components
        - Rotates the axis and calculates the across- and along-shore wind speeds
        - Averages all data by day
        - Calculates a daily Ekman Transport as a proxy for upwelling index
    - Because physical data measured at the buoys are highly correlated, we used regression equations relating the San Francisco buoy and Half Moon Bay buoy data to the Bodega Bay buoy data to fill-in data gaps for each variable (sea surface temperature, alongshore wind speed, across-shore wind speed, and upwelling indices). Using the regression equations with the best R^2 values, missing Bodega Bay buoy data are filled in.
    - Monthly averages are calculated for each year, as well as monthly averages over the long-term time series (1981-present).
    - Monthly anomalies are calculated by subtracting the long-term monthly average from the monthly average calculated for that year.
    - 99% confidence intervals are calculated based on the long-term monthly averages.
    - For the spring transition figure (Figure 11):

- Cumulative upwelling values are calculated based on the daily upwelling index.
- The first date of a sustained upwelling event in the spring of each year is defined as the spring transition date.
- The long-term mean (1981-present) in spring transition dates is subtracted to obtain annual anomalies.
- 99% confidence intervals are calculated based on the long-term mean in spring transition date.

NOAA Pacific Fisheries Environmental Laboratory (PFEL) Coastal Upwelling Indices

- *Source*:
  - https://oceanview.pfeg.noaa.gov/products/upwelling/dnld
  - Monthly and daily upwelling indices calculated based upon Ekman's theory of mass transport due to wind stress (for more information, see their website: https://oceanview.pfeg.noaa.gov/products/upwelling/intro).
- Data used in Figures 8 and 10.
- *Data processing*:
  - Since our study area is situated between two upwelling index locations, monthly and daily upwelling indices (1946-present) are downloaded for two locations (36N 122W and 39N 125W), and an average monthly upwelling index and a daily upwelling index is calculated between these two locations.
  - The average monthly upwelling indices are then averaged by month for the entire time series (1946-present) to obtain the long-term monthly averages.
  - The long-term monthly averages are subtracted from the monthly upwelling index to obtain the monthly anomalies.
  - 99% confidence intervals are calculated based on the long-term monthly means.
  - For the spring transition figure (Figure 10):
    - Cumulative upwelling values are calculated based on the average daily upwelling index.
    - The first date of a sustained upwelling event in the spring of each year is defined as the spring transition date.
    - The long-term mean (1972-present) in spring transition dates is subtracted to obtain annual anomalies.
    - 99% confidence intervals are calculated based on the long-term mean in spring transition date.

Coastal Upwelling Transport Index (CUTI)

- *Source*: http://mjacox.com/upwelling-indices/
- Data used in Figure 9.
- *Data processing*:
  - A daily upwelling indices file is downloaded. Indices are provided in 1° latitude bins (ranging from 31°N to 47°N); a daily average of the 37°N and 38°N values is calculated to best represent our study area.
  - The 37-38N daily upwelling indices are then averaged by month for the entire time series (1988-present) to obtain the long-term monthly averages.

- The long-term monthly averages are subtracted from the monthly upwelling indices to obtain the monthly anomalies.
- 99% confidence intervals are calculated based on the long-term monthly means.

Farallon Island sea surface temperature and salinity data

- *Source*: https://shorestations.ucsd.edu/data-farallon/
- Data used in Figures 13 and 15.
- *Data processing*:
  - The updated Excel files are downloaded from the website.
  - Monthly averages of SST and SSS are calculated for each year, as well as monthly averages over the long-term time series (1925-present).
  - Monthly anomalies are calculated by subtracting the long-term monthly average from the monthly average calculated for that year.
  - 99% confidence intervals are calculated based on the long-term monthly averages.

Chlorophyll a, sea surface temperature, and sea level height satellite data

- *Source*: https://oceancolor.gsfc.nasa.gov/cgi/l3
  - Data are downloaded using the Marine Geospatial Ecology tools through ArcGIS. The bounding coordinates are 39 -124, 37 -122 (N & W, respectively).
  - Chlorophyll a data are from the NASA GSFC OceanColor Group and include data from two different satellites: SeaWIFS (9 km resolution), which was discontinued in 2010; and MODIS Aqua (9 km and 4 km resolution).
  - Sea surface temperature data are from NASA JPL PO.DAAC and include data from the MODIS Aqua satellite (4 km resolution).
  - Sea level height data are from the AVISO satellite (1/4 degree).
- Data used in Figures 6, 14, and 21.
- *Data processing*:
  - For chlorophyll a, monthly mean abundance (in mg/m^3) from SeaWIFS is used for the early years (Sep 1997-Dec 2004), then Aqua data are used for 2005 - present. Long-term (1997-present) monthly means, standard deviations, and counts are calculated. Monthly anomalies are calculated for years 2004 - present by subtracting the long-term monthly mean from the monthly mean. 99% confidence intervals are based on the long-term monthly standard deviation and the number of data points for that month.
  - For sea surface temperature, the monthly mean temperature (in °C) from Aqua is available for Jul 2002–present. Long term (2002-present) monthly means, standard deviations, and counts are calculated. Monthly anomalies are calculated for years 2004-present by subtracting the long-term monthly mean from the monthly mean. 99% confidence intervals are based on the long-term monthly standard deviation and the number of data points for that month.
  - For sea level height, the monthly mean sea level height (in m) from AVISO is available for Jan 2002–present. Long term (2002-present) monthly means, standard deviations, and counts are calculated. Monthly anomalies are calculated for years 2004-present by subtracting the long-term monthly mean

from the monthly mean. 99% confidence intervals are based on the long-term monthly standard deviation and the number of data points for that month.

ACCESS data

Below are descriptions of the data collected from the ACCESS cruises.

Conductivity-temperature-depth (CTD) recorder data

- Data used in Figures 16 and 17.
- Hydrographic data are collected with a Sea-Bird Electronics (SBE) CTD instrument. In most cruises, we use a SBE 19plus SeaCAT Profiler CTD, which is fitted with a SBE 5T submersible pump, WETStar fluorometer, Campbell backscatterance sensor, and a SBE 43 oxygen sensor (added in 2010); however, a SBE 19plus SeaCAT Profiler CTD (fitted with a WETStar fluorometer) and a SBE 9+ CTD (fitted with a SBE 43 oxygen sensor and WETlabs FLNTU fluorometer) were used on certain cruises. The CTD is lowered at a rate of 30 m/min down to either 200 m (at deeper stations) or within 10 m of the bottom (at shallower stations). The CTD was lowered to 1000 m depth over the Davidson Seamount area.
- Downcast data are processed with the SBE Data Processing v7.2 application, and through a series of data processing steps, 1 m-binned averages are produced of each hydrographic variable; these variables are pressure (psi), temperature (°C), conductivity (S/m), fluorescence (mg/m^3), backscatterance (ntu), dissolved oxygen (mg/L), percent oxygen saturation, density (kg/m^3), and salinity (psu).
- For aragonite saturation state (Figure 16):
    - The 1 m-binned data on salinity, temperature, and dissolved oxygen are used in a regionally specific empirical equation developed by Davis *et al.* 2018 to calculate the aragonite saturation state with each CTD cast.
    - Since the dissolved oxygen sensor was installed in 2010, no aragonite saturation state values can be calculated for the early years (2004 - 09).
    - Only CTD casts for July cruises, line 2, station W were used to create the figure.
    - A Jupyter Notebooks script is used to generate interpolated figures.
- For dissolved oxygen (Figure 17):
    - The 1 m-binned data on dissolved oxygen concentrations for CTD casts on July cruises (line 2, station W) were used to create the figure.
    - Since the dissolved oxygen sensor was installed in 2010, no dissolved oxygen concentration values are available for the early years (2004-09).
    - A Jupyter Notebooks script is used to generate interpolated figures.

Surface water nutrients

- Data used in Figures 18, 19, and 20.
- Seawater samples in the top 0-1 m are collected with a polyethylene bucket. The bucket is tossed overboard three times, with the first two bucket collections being poured out to rinse the bucket of previous surface collections; water from the third toss is collected for analysis. Water is poured into a 20 mL polyethylene scintillation vial and emptied twice; on the third pour, the vial is filled approximately two-thirds full, capped, and labeled. Samples are stored upright in a freezer and kept in dark conditions until transferred to the Frances Wilkerson Laboratory at the Estuary and

Ocean Science Center (San Francisco State University's Romberg Tiburon Campus, Tiburon, CA) for analysis.

- Samples are defrosted 24 hours prior to analysis to mitigate silicate polymerization effects (Macdonald *et al.* 1986) and analyzed with a Bran and Luebbe AutoAnalyzer II colorimeter with MT-19 manifold chemistry module using standardized automated techniques. Nutrients in each sample are reduced using a series of chemical reactions and dyed to be recognized by the colorimeter. Nitrate+nitrite (NO_3 + NO_2) are analyzed according to Whitledge *et al.* (1981) and Bran and Luebbe Inc. (1999a) Method G-172-96, phosphate (PO_4) according to Bran and Luebbe (1999b) Method G-175-96, and silicate ($Si(OH)_4$) by Bran and Luebbe Inc. (1999c) Method G-177-96.

Phytoplankton species composition data

- Data used in Figure 22.
- Samples are collected with a hand-held net (25 cm diameter, 1 m length, 20 µm mesh), which is vertically towed in the upper 10 m of the water column three times (for a total of 30 m).
- Samples are analyzed by the Biotoxin Monitoring Program. Data provided are qualitative and include percent composition of each species identified, which is the species relative percentage to all other species present in the sample.
- Monthly average percent composition is calculated for diatoms and dinoflagellates from the offshore samples only. Note that the figure only includes diatoms and dinoflagellates, but other organisms (e.g., ciliates, copepods, foraminifera) are not reflected here.
- Averages over the two periods (March-July and August-February) are calculated.

Zooplankton data

- Data used in Figures 23, 24, 25, 26, 27, 28, 30, and 31.
- We sample zooplankton using a hoop net and a Tucker trawl:
    - The hoop net is a 1 m-diameter net equipped with a 333-µm mesh and a General Oceanics 2030RC mechanical flowmeter (to measure volume of water sampled). All samples collected in the upper 50 m of the water column and provide information on zooplankton composition.
    - The Tucker trawl has a ~1 m^2 net opening and furnished with three nets and a 333 µm mesh; the opening of each net was outfitted with a flowmeter (General Oceanics, model 2030RC) to record the volume of water filtered during each net tow. A double release mechanism was attached to the net's cable; chains attached to the mechanism and the nets could be triggered to release (thereby closing one net and opening the next net) with 1 kg bronze messengers sent down the net's cable, allowing for sampling at three different depth strata (with the deepest net sampling 200 m or deeper). The Tucker trawl data provide information on krill (e.g., abundance, species composition, and age classes).
- All zooplankton samples are saved in seawater and fixed with formalin.
- All hoop net samples are then sent to Moira Galbraith (Institute of Ocean Sciences, Sidney, British Columbia), where all organisms are identified to the lowest taxonomic level possible. In brief, entire samples are scanned for large and/or rare taxa using a Wild M420 dissecting scope with 20x oculars and varying zoom objective (10-30x),

depending on the contents of the sample. Using a Folsom splitter, the sample is quantitatively subsampled for counts of small abundant zooplankton taxa. Total counting effort is ≥400-500 individuals per sample, sufficient to give an expected subsampling error of ≤20% for the dominant species (Mackas and Galbraith 2002, Mackas *et al*. 2005, Postel *et al*. 2000). Euphausiids are identified to species (when possible) and age class (egg, zoea, juvenile, immature female and male, and adult female and male), and then measured and weighed. Numbers of euphausiids (by species, age class, and size class) for each sample are compiled, entered into a Microsoft Excel file, and emailed to Point Blue.

- Tucker trawl samples are analyzed in the Point Blue laboratory in Petaluma. After draining off the formalin, the sample is weighed and biovolume estimated. Large specimens (>5 cm) are removed, and the sample is transferred to a Folsom splitter. The sample is split until an aliquot containing 80-100 euphausiids (zoea through adult stage) is obtained. Using either a National Optical DC5-420TH digital microscope (with either 10x or 20x oculars and varying zoom objective (10-40x)) or an AmScope ZM-2TZ trinocular zoom microscope (with 10x oculars and varying zoom objective (10-40x)), euphausiids are identified to species (when possible) and age class (zoea, juvenile, immature female and male, and adult female and male), and then measured and weighed. Numbers of euphausiids (by species, age class, and size class) for each sample are compiled.
- Abundances of taxonomic groups in a sample are calculated by the number of individuals of a taxon divided by the volume of water sampled.
- For Figures 23, 25, 26, 27, and 28: Average abundances of taxa in hoop net samples are calculated by cruise, using only samples collected from lines 2, 4 and 6 (see Figure 1), as these lines were surveyed in all years.
- For Figure 24: Zooplankton abundance data from each hoop net sample are analyzed in Primer 7 (Clarke & Gorley 2001) using a non-metric multi-dimensional scaling analysis (NMDS) to understand similarities between samples (Clarke 1993); NMDS analysis is restricted to samples collected in spring and summer months (April-July) to remove seasonal effects and increase the robustness of the results.
- For Figure 30: Using *Euphausia pacifica* data from Tucker trawl samples, we summed the wet weights of each age class in each sample, then summed the wet weights of each age class for a cruise. Percentages of each age class were calculated based on the total wet weight of *Euphausia pacifica* in each cruise.
- For Figure 31: Using adult *Euphausia pacifica* size data from Tucker trawl samples in spring/summer samples (May-July), the total number of adults in each size class were summed for a year. Percentages were either based off of total number of *E. pacifica* adults identified in samples that year or range of years.

Hydroacoustics data

- Data used in Figures 29 and 51.
- Each research vessel utilized in ACCESS cruises was equipped with a multi-frequency Simrad EK 60 split beam echosounder with a transducer array of 38, 120, and 200 kHz. Krill were sampled every 2 seconds along transect lines.
- Raw volume backscatter data were post-processed. Using Echoview software (Sonardata, Pty. Ltd.), krill biomass was integrated into 200 m horizontal by 5 m depth bins, which excluded the surface layer (0-5 m) to avoid surface interference.

- The sum of all krill biomass down to 200 m was summed for each cruise for the core area (lines 1-7; see Figure 1).

Bird and mammal observations

- Data used in Tables 1 and 2, and Figures 32, 33, 37, 38, 42, 43, 47, 48, 49, 50, 51, and 52.
- Bird and mammal observations were collected during each ACCESS cruise from the vessel flying bridge using standardized strip-survey methods. Observations were recorded while on effort, which is defined as transiting a transect line with an observer actively recording bird and mammal observations during daylight hours and vessel speed of ~10 knots. Birds were observed by an observer within a 90° arc from the bow to the vessel's starboard side and within 50-300 m of the vessel, while mammals were observed by two observers covering a 180° arc from port to starboard and out to the horizon. Data on factors that affect detection (e.g., sea state, visibility, cloud cover) were also noted.
- Transect lines were subdivided into 3 km bins, and counts of birds and mammals were assigned to these 3 km bins.
- Abundances of bird species (i.e., number of animals observed per km^2 of survey area) observed on lines 1-10 were summarized over the time series (2004-present; Table 2). Abundances of important seabird species were further summarized by cruise (Figures 32, 37, and 42), and spatial distributions were plotted for the month of May or June of each cruise (Figures 33, 38, 43).
- Abundances of mammal species (i.e., number of animals observed per km of survey distance) observed on lines 1-10 were summarized over the time series (2004-present; Table 3). Abundances of important whale species were further summarized by cruise (Figures 47 and 49), and spatial distributions were plotted for each month of each cruise (Figures 48 and 50).
- Figure 51: Blue whale abundance (calculated as number of individuals per km^2) for lines 1-7 is shown here.
- Figure 52: Humpback whale abundance (calculated as number of individuals per km^2) for lines 1-7 is shown here.

Southeast Farallon Island seabird data

For information on seabird data collected from the Farallon Island, please refer to:

Johns ME, Warzybok P. 2019. Population size and reproductive performance of seabirds on Southeast Farallon Island, 2019. Unpublished report to the U.S. Fish and Wildlife Service. Point Blue Conservation Science, Petaluma, California.